IMPROVEMENT OF A DETECTION SYSTEM FOR *IN-VIVO* AL MEASUREMENTS, AND *IN-VIVO* AL MEASUREMENTS OF A POPULATION OF MINERS

IMPROVEMENT OF A DETECTION SYSTEM FOR *IN-VIVO* AL MEASUREMENTS, AND *IN-VIVO* AL MEASUREMENTS OF A POPULATION OF MINERS

By: LAURA BICKLEY B.Sc.

A Thesis Submitted To The School Of Graduate Studies

In Partial Fulfilment Of The Requirements For The Degree Master Of S

M.Sc. Thesis - Laura Bickley; McMaster – Radiation Sciences (Medical Physics)

McMaster University MASTER OF SCIENCE (2020) (Radiation Sciences – Medical Physics)

Hamilton, Ontario, Canada

Title: Improvement of a detection system for *in-vivo* Al measurements, and *in-vivo* Al measurements of a population of miners.

Author: Laura Bickley B.Sc. (University of Guelph)

Supervisor: Dr. David Chettle, Dr. Fiona McNeill

Number of Pages: x, 70

Abstract:

The following thesis seeks to investigate potential alternatives to the 4π system employed by the Tandem Accelerator Laboratory (TAL) at McMaster University for use in the investigation of in-vivo aluminum levels using *in-vivo* neutron activation analysis. It also aims to measure the levels of aluminum in miners who were exposed to it via inhalation of the Aluminum containing McIntyre powder from ~ 1944-1979.

The same protocol for creation and irradiation of phantoms was followed as in [1], namely tissue equivalent phantoms were created and irradiated under a proton current of 400 μA, with a proton energy of 2.3 MeV which led to neutron energies of 0.55 MeV. These phantoms were then counted using three different detectors. These detectors consisted of two scintillators (the currently used 4π NaI(Tl) system, and a single LaBr3(Ce)) and a semi-conductor, a single closed-end coaxial HPGe. MDLs for these detectors were found to be 15.85 μgAl/gCa (236.17 μgAl) for the 4π NaI(Tl) system, 56.51 μgAl/gCa (842.0 ugAl) for the HPGe and 98.67 μgAl/gCa (1470.20 μgAl) for the $LaBr_3$(Ce).

The next part of the thesis involved in-vivo measurements on a group of 15 miners from Northern Ontario who had been exposed to McIntyre powder previously throughout their careers in the mines. Each patient was irradiated under the same proton current and energy as above, and was transferred to the 4π system for counting for 10 1 minute cycles. The MDL for these in-vivo measurements was found to be 22.57 μgAl/gCa. The highest value was 206.36±14.76 μgAl/gCa and the lowest value was 18.55±3.95 μgAl/gCa, with a median value of 18.56±11.28 μgAl/gCa and average value of 21.78±2.27 μgAl/gCa for IVWM, and 17.43±13.78 μgAl/gCa for regular mean. Of the miners, 7 had negative concentrations, indicating that the concentrations were below the detection limit of the system.

Data analysis for all experiments was performed the same way. The Al/Cl peak for the NaI was fit using a FORTRAN algorithm, as well as the Ca peak. The areas for these peaks were then calculated, then the MDL was calculated by taking the average of the low concentration phantoms, and the error was multiplied by 2, then was divided by the calibration slope for the first three time cycles. These values were then added via the inverse variance weighted mean (IVWM) method, and the final concentration of μgAl/gCa was calculated.

Given that the HPGe had a significantly better MDL than the $LaBr_3$(Ce) (56.51 vs 98.67 μgAl/gCa), that the HPGe may be a good candidate to improve the current 4π in-vivo system. Also given the high amount of Al found in the bones of the miners, this indicates that it can be a good indicator of how much Al each miner was exposed to and may help with assessing the health effects of McIntyre powder.

Acknowledgements:

Thank you to Drs. David Chettle and Fiona McNeill for supervising me, providing their excellent guidance, and putting up with my constant delays, Dr. Byun for being on my committee and allowing me to use his $LaBr_3$(Ce) detector and electronics equipment as well as his help with the solid angle calc., Justin Bennett for running, fixing and maintaining the accelerator, Janice Martell, Kevin Hedges, and all the people involved with OHCOW and the McIntyre powder project for coordinating the participation of the miners, Dr. David Cowan for assessing the miners, Kenrick Chin for implementing the auto-calibration, and Benjamin Price for helping run the Tandetron, as well as helping with the *in-vivo* study. I would also like to thank my parents, David and Cathy for helping to keep me somewhat sane during my writing, as well as all my friends.

Table of Contents

List of Tables

List of Figures

Chapter 1: Introduction

1.1 Aluminum in the environment

Aluminum is the 2nd most abundant element, and most abundant metal in the earth's crust. Aluminum is very reactive, combining with elements such as oxygen, fluorine and silicon.It has been found in many plant species and is used in a wide variety of applications such as water filtration, utensils, pop cans, cosmetics and medication. It also has wide applications in cosmetics and food additives [7]

1.2 Aluminum in the body

Aluminum in the body is a different story. Due to its abundance there is a small amount of aluminum present normally in humans. One method of assessing Al exposure is measurement in serum: the number is approximately 5μg/L in plasma. [5]. However, while everyone is exposed to a small level of aluminum, there are risks with heightened aluminum exposure. In dialysis patients, conditions such as encephalopathy and osteomalacia were observed for patients exposed to dialysis fluids that contained aluminum [6], or from pumps that contained aluminum [20], and cases were reported to decrease when the aluminum was taken out of the fluids [6].

In the 70s there was an outbreak of encephalopathy in Denver, this was thought to be due to aluminum in both the dialysis fluid and the Al given to patients to control the level of phosphate in their blood serum [21] .

In another reported study [18], patients receiving parenteral nutrition for loss of small bowel function were found to have bone pain and fractures that were not caused by injury. None of these patients had impaired renal function. Bone biopsies were taken and it was reported that

aluminum was present in them, while for a control group no aluminum was found. In the patients where aluminum was present, bone formation was decreased as well as uptake of Vitamin D.

While vitamin D metabolism seemed to be affected, further studies were needed to confirm this. When one patient was taken off the aluminum containing compound, their bone formation went up, and the total bone aluminum levels went down, suggesting that the Al was the cause of this altered metabolism. [18]

In 2005 [3] cases of hyperaluminea (excess aluminum levels) were reported in Canadian peritoneal disease centres. While there were no obvious health consequences for those exposed to aluminum, most likely due to the quick response of physicians, those patients that were exposed to aluminum longer had higher blood serum aluminum levels than those who were exposed for less amounts of time, suggesting that the longer someone is exposed to aluminum the more it can accumulate in serum. It should also be noted that for those patients with a lower kidney clearance rate, aluminum levels were higher.

1.3 McIntyre Powder

Before the introduction of McIntyre powder one of the most prevalent diseases among miners was silicosis of the lung. This was caused when miners would work underground and inhale silica dust, in order to combat this, reports were published in the 1930s, theorizing that aluminum may be able to bind to the silicon, thus preventing the disease. [23]

McIntyre powder first came into use in 1943, and was estimated to have affected 27,500 miners throughout its use until it was discontinued in 1979 [25]. Chemically, the powder contained 15% elemental Al and 85% aluminum oxide, the recommended exposure was 20000-34000 ppm of air.

Miners had to inhale the powder before every work shift, where they were placed in a self-contained room, into which the dust was pumped. They were required to stay in the room for 10 minutes, which resulted in an exposure of 35.6 mg Al/m^3 [19]

In the 50s a new type of McIntyre powder was formulated, this contained 13% metallic aluminum, with particle sizes from less than 1.2 μm, while the rest of the powder had particles sizes 400 nm in diameter. [19]

A small study of 8 autopsied lungs from miners exposed to McIntyre powder was conducted. Measurement of levels of Al in lung was conducted in addition to measuring the lungs for levels of Ni, Cd and Pb. The study was done to have a published record of the amount of aluminum in the lung of miners exposed to McIntyre powder. The lungs showed elevated levels of aluminum with a mean of 476.4 micro gram aluminum per gram dry tissue, compared to 158.4 μgAl for urban non-McIntyre powder-exposed lung in humans and a mean of 36.6 μgAl from a pig control.[24]

With this observed lung exposure there comes the question of what, if any, health effects the inhalation and subsequent retention of this powder in lung could cause. A study of Cornish miners [25] who worked in tin mines between 1941 to 1984 found no association between exposure to McIntyre powder and Alzheimer's Disease, though by the authors' admission the small sample size, and the known issues with accuracy of historical death certification, could be limiting factors in the validity of this conclusion. Yet another paper [9] looked into the potential association between Alzheimer's Disease and McIntyre powder. A group of 647 miners who were exposed to McIntyre powder from 1940 to 1959 were selected from an initial group of 6604

to be investigated. Reasons for the small percentage of miners selected were due to many reasons, including not being able to contact miners, miners not completing survey requirements, and death.

One subject had a ‘probable’ diagnosis of Alzheimer’s, 3 had Parkinson’s and another had a ‘probable’ diagnosis of Alzheimer’s given by proxy.

Each subject was given three cognitive tests to assess impairment (MMSE, CPM, SDMT). Any subjects with previous neurological conditions or head trauma were excluded. The test results were summed and plotted against time in the mines. The exposure to aluminum was compared against time underground, with a positive correlation resulting. [9]

The summed test scores seemed to indicate a negative correlation with exposure time, implying that the exposure to aluminum could have contributed to impaired cognitive function. Though as pointed out in [25] the authors did not provide justification for summing the three scores, nor did they normalize the data. In addition, the small percentage of miners included in the study may result in selection bias. Another issue present is the Al levels in bone were not actually confirmed via bone biopsy, or IVNAA, instead choosing to use the levels reported from annual chest examinations. However, since they did not look at aluminum body burden it is still unclear if the aluminum was the underlying cause of the observed health effects and potentially warrants further investigation.

1.4 Measurement of Aluminum

In order to look at levels of aluminum in humans there are two options. To measure acute aluminum exposure aluminum blood serum levels are generally taken. However, this may not provide an accurate measurement of long-term exposure, for this bone is looked at instead. [1]

Traditionally to look at the body burden of aluminum bone biopsies are taken [1] These can be extremely painful for the patient, and so non-invasive techniques were sought out. One such technique was in-vivo neutron activation analysis, first done by [22] in 1980. Neutron activation analysis permits the low risk, non-invasive assessment of aluminum content in bone. In this technique neutrons are directed at a target, and subsequently a neutron can be absorbed creating an isotope of the same element with an increase in atomic mass of one. If this isotope is radioactive, or if the product isotope is in an excited state, it can then de-excite emitting a gamma ray that can be measured with various detectors. For aluminum, the reaction generally used for in vivo measurement is $^{27}Al(n,\gamma)^{28}Al$, with a cross section of 0.23 barn. ^{28}Al has a half-life of 2.24 minutes, with a gamma emitted for each decay to ^{28}Si.

The choice of neutron source also plays a role in measuring aluminum in-vivo. There are two competing reactions that can produce ^{28}Al and hence result in the emission of the same characteristic gamma rays. These reactions are $^{31}P(n,\alpha)^{28}Al$ and $^{28}Si(n,p)^{28}Al$. Both elements are found in significant amounts within the human body and thus are potentially significant interferences in the assessment of aluminum. In a previous study [26] these reactions caused interferences as the ^{252}Cf neutron source used in the study emits high energy neutrons and thus the interference from both reactions had to be taken into account.

In [1], however the Tandetron accelerator was utilized. Being able to accurately control the energy of incident neutrons emitted from the source is an important advantage when measuring aluminum in-vivo using the Tandetron accelerator. The Tandetron is a 1.25 MV tandem accelerator from HVL in the Netherlands, and can accelerate protons up to energies of 2.5 MeV. The Tandetron has the ability to control the energy of the accelerated protons, and thus the energy of the created neutrons. Per [1] the maximum neutron energy produced by irradiation of a

lithium target is 0.55 MeV for 2.3 MeV protons. Since the reactions $^{31}P(n,\alpha)^{28}Al$ and $^{28}Si(n,p)^{28}Al$ have energy thresholds of 2.007 MeV (^{31}P) and 3.985 MeV (^{28}Si) respectively, both are well above the incident 0.55 MeV energy. These competing and interfering reactions can thus be eliminated from the measurement.

In the human body the following elements have neutron absorption cross sections within the thermal neutron energy range and can produce observable gamma rays: the reactions are $^{48}Ca(n,\gamma)^{49}Ca$, $^{23}Na(n,\gamma)^{24}Na$, $^{37}Cl(n,\gamma)^{38}Cl$, and $^{26}Mg(n,\gamma)^{27}Mg$

^{24}Na has a half-life of 14.95 hours, and decays by beta minus emission 100% of the time. The two most prominent gammas it emits are at 1368 keV (100%), and 2754 keV (99.944%). It also emits other gamma rays, but these are all <1% of the time so will not show up very strongly on a spectrum and thus can be ignored. [27]

^{27}Mg has a half-life similar to that of ^{49}Ca at 9.458 minutes. It decays by beta minus emission 100% of the time. The most prominent gamma rays it emits are at 844 keV (71.8%) and 1014 keV (28.0%) while a third gamma is emitted at 171 keV (0.8%). [27]

Two reactions of particular note are the reactions of Ca, $^{48}Ca(n,\gamma)^{49}Ca$, and Cl, $^{37}Cl(n,\gamma)^{38}Cl$. The Ca reaction produces two gamma-rays (one of energy 3.08 MeV 92% of the time and the other at ~4.0 MeV ~7% of the time) [27]. It decays exclusively by beta minus decay, with a half-life of 8.718 minutes. The 3.08 MeV is sufficiently isolated in energy so as to not overlap with any other gamma rays of elements present in the human body. This calcium feature is useful and is used to normalize the aluminum concentration to the calcium concentration in the human body. This makes the accuracy of the measurement independent of bone shape, size, mass or

density. The precision can, of course, vary with these factors. Other gamma rays are produced by the $^{48}Ca(n,\gamma)^{49}Ca$ reaction, however the percentages are all <1%.

The second gamma-ray produced by the $^{48}Ca(n,\gamma)^{49}Ca$ reaction is of energy 4.05MeV.The other reaction is the Cl reaction. This produces two gamma -rays. Of particular interest is that one is of energy 1.64 MeV. This gamma-ray is extremely close to the 1.78 MeV gamma ray produced by the Al reaction. This presents a problem in the case of the sodium iodide detector, which cannot completely resolve the two peaks. Cl also has another neutron capture reaction, that of $^{35}Cl(n,\gamma)^{36}Cl$, though ^{36}Cl has a half-life of 300,000 years, and will not contribute much to the spectrum, and therefore can be ignored. [27]

This 1.64 MeV Cl gamma-ray causes an issue for in-vivo studies as chlorine is found in much higher abundance in the body than aluminum, resulting in the chlorine peak being significantly taller than the aluminum peak. This engulfs the smaller aluminum peak. While spectral deconvolution of the spectrum, or alternatively only fitting relevant regions with a double Gaussian, has been used to help decrease the uncertainty introduced by this gamma-ray, this can still contribute to increasing the uncertainty of the area under the curve and thus worsening the precision of aluminum measurement.

When a radioactive isotope emits multiple gamma rays during its decay, the timing between when each of these photons reaches different detectors can be utilized. A timing window is selected and if two photons enter detectors within this time frame, it is counted as from the same source and counted, this is called coincidence [35,36]. The opposite is anti-coincidence, where if two photons are counted within the same time window, they are not counted and thus are not added to the spectrum [36]. The latter is used for the ^{38}Cl gamma rays in order to minimize their

contribution to the spectrum, and thus minimize how much the 1.64 MeV photon interferes with the 1.78 MeV photon from ^{28}Al [12].

1.5 Scintillator Detectors

1.5.1 General Properties

Scintillator detectors are adapted from naturally scintillating materials. In a crystal scintillator, when a photon interacts it leads to an excitation of an electron within the crystal structure from the ground state in the valence band to an excited state. The electron then decays back to the ground state, releasing a photon of the energy difference between the valence and excited states. If the crystal is pure the process is not very efficient as the band gap is relatively large, meaning the electrons need a much greater energy in order to be raised to the excited state ultimately releasing photons during their de-excitation. To compensate for this, impurities, called activators, are added to the crystals. These activators create excited states within the band gap. Electrons can be more readily excited to these multiple activator excited states and this leads to the release of photons in the visible light spectrum. These photons do not have enough energy to cause excitations within the normal crystal structure, and thus the detector material is transparent to them. These visible photons can thus be detected outside of the crystal. [10]

This emitted light is converted to photo-electrons, by interaction with a photocathode, and the electric signal is amplified via dynodes in a photo-multiplier tube (PMT) to create a detectable signal. [10,11]

The resolution of a scintillator detector is affected by three things: the intrinsic crystal resolution, the PMT characteristics and the probability of a photon being collected at the dynode (called the transfer variance). The intrinsic crystal resolution can result from localized fluctuations in the

crystal efficiency, in modern practice this is not a significant contributor to the overall resolution, contributing at most 2%. [10] Characteristics can vary between different PMTs, with some having non-uniform photon collection, resulting in a broadening of the peak, and worsened resolution. If the transfer variance is low and few photons are collected at the dynode then this can also cause a decrease in resolution. The variance for N dynodes is given by $\sigma^2 = \frac{1}{\delta - 1}$ where δ is the amount of electrons produced per dynode. If the amount of electrons produced is small, then the variance will become larger, thus broadening the peak [13].

There is also a non-linearity in the response of crystals. This arises when a gamma ray's energy is split between two or more different electrons. Even if the gamma-ray source is mono-energetic a wide array of electron energies has been observed. The reason for this is due to how electrons are produced when photons interact with matter, create electrons and lose energies. There are multiple ways that photons can interact with matter, two such processes that are common are the photo-electric effect (where the photon transfers all its energy to an electron) and the Compton effect, where the energy distributed to the electron depends on the angle of the incident photon. These different methods of interaction cause differences in the loss of electron energies, which in turn causes different energy electron energies to be produced, which can increase variance, and can cause a mono-energetic photon to appear as if it is spread over a continuum of energies. The system cannot differentiate between these two different types of electrons, and therefore reads them as different energies. [13]

Efficiency in crystals depends on energy, dropping off with higher energies as higher energy particles tend to lose less energy compared to lower energy particles. Due to ease of manufacture, almost all crystals have the same properties when it comes to radiation interactions, and can be produced with virtually identical properties. [10,11,13]

1.5.2 Sodium Iodide

Sodium iodide detectors are widely used as they are both highly efficient and relatively inexpensive compared to other types of detectors, or other scintillators. They also do not need to be cooled by liquid nitrogen as is necessary with semi-conductor detectors. However, one major drawback to the sodium iodide detector is its resolution. Previous studies measuring aluminum in bone have utilized thallium doped sodium iodide crystals, NaI(Tl)as the detectors [1,2,28,26] The configurations have ranged from two detectors to an array of nine.

While the most common and cheapest type of scintillator detector is NaI(Tl), there are alternatives. Scintillators come in multiple different types; other crystals include BGO, and $LaBr_3$(Ce).

1.5.3 Lanthanum Bromide

Cerium doped lanthanum-3-bromide detectors ($LaBr_3$(Ce)) are scintillators like sodium iodide. Compared to NaI(Tl), $LaBr_3$(Ce) detectors are faster, more efficient and have a better resolution (3% at 662 keV, compared to 6 or 7% for NaI(Tl)). However, sodium iodide detectors have a much larger light yield, and the proportionality of light intensity to the number of photons decreases for lower energies (<20keV) for the $LaBr_3$(Ce). This loss of proportionality can lead to a poorer resolution and loss of events. Another drawback to the lanthanum detectors is that one isotope of lanthanum is radioactive and there is thus a 1436 keV gamma from ^{138}La, as well as alphas from contamination of ^{226}Ac inherent to the crystal. The ^{138}La peak overlaps with the commonly observed 1460 keV room background peak from ^{40}K. [4]

In studies [8], lanthanum bromide showed many more peaks at higher energies than lower energies compared to sodium iodide. The same study also found a reduction in relative

background levels for $LaBr_3$(Ce), leading to an improvement in signal-to-noise ratio (SNR) of 25 to 35%, with maximum count rates being 3 to 47% higher for $LaBr_3$(Ce). [8]

The improvement in resolution should also have an impact on the uncertainty of the aluminum concentration. In theory it should decrease the uncertainty in the aluminum measurement as the overlapping chlorine peak will be resolved from the aluminum peak. In addition, the total background signal under the aluminum peak may be smaller, because it is narrower. As minimum detectable limits (MDLs) should vary with the square root of the background signal, it is possible that better MDLs can be obtained.

1.6 Semi-Conductor Detectors

Semi-conductor detectors operate by taking advantage of the properties of natural semi-conducting materials. For a given material to be a semi-conductor there needs to be a band-gap between the valence and conduction band of a few eV. If the band-gap is greater than 5 eV then no electrons can flow by being thermally excited to the conduction band at normal room temperature, therefore no current is created; this is called an insulator. The opposite case, where there is almost no band-gap between the conduction and valence bands and electrons can flow freely is called a conductor. A semi-conductor lies in the middle.

Materials such as germanium and silicon act as intrinsic semi-conductors, however the use of dopants can greatly amplify the efficiency of the semi-conductor. Both silicon and germanium are tetravalent (group IV in the periodic table, possessing four valence electrons). To create an n-type semiconductor small amounts of pentavalent impurities are added so that they replace a silicon (or germanium) atom within the crystal structure. Since the impurity has 5 valence electrons (due to it being from group V of the periodic table, or pentavalent), an extra electron is

present, not strongly bound to the original impurity atom. Due to this the extra electron is quite easy to dislodge. These impurities are therefore called donor impurities as they readily donate their extra electron. These impurities form n-type semiconductors. P-type semi-conductors utilize acceptor impurities (group III, trivalent). These impurities have one less valence electron than the silicon, creating an electron hole that readily accepts outside electrons.

The impurities are added in sufficiently low concentrations, so any interactions with incoming radiation is negligible [13]).

For a semi-conductor to function as a detector, a junction is formed between a p-type and n-type semiconductor (called a p-n junction). This is formed when either a p or n-type semiconductor is brought into thermal contact with the opposing type. The junction acts as a discontinuity in the electron density, causing the holes and electrons to diffuse from the high density side to the low density side. This causes a net negative charge on the p type side and a net positive charge on the n-type side.

This causes an imbalance in charge density, creating what is called the depletion region. This also causes an electric potential to be created over the depletion region. In this region photons can interact, creating electron-hole pairs that will be swept either towards the positive or negative side of the detector. The ionization energy is small (3eV needed per pair for Ge compared to 30eV per pair for a gas detector), meaning more electron hole pairs, and therefore a larger signal can be produced. The induced electric field in the depletion region, however, is too weak to efficiently collect the created holes and electrons, therefore a large voltage is applied in order to reach drift velocity, usually around 10^7cm/s. As the voltage is applied the depletion region grows, and more events can be detected [13,10].

Silicon has a much smaller depletion depth compared to germanium of less than 1mm, making it good for soft x-ray detection [13,10]. In order to detect photons in the MeV range a depletion region of 5cm is sufficient, this is the depletion region depth for germanium.

Germanium also has another advantage over silicon as it has a higher linear attenuation coefficient, meaning higher energy photons that may pass through silicon have a higher chance of interacting with the germanium and therefore being detected [13].

However, the semi-conductor detectors do not have as high an efficiency as the scintillator detectors. This means a potential loss of signal which could lead to an increase in the uncertainty of the aluminum measurements and hence a poorer detection limit.

1.6.1 HPGe Detectors

HPGe detectors have extremely high resolution (2keV at 1332 keV) compared to both the $LaBr_3$(Ce) and NaI(Tl) detectors, but have a much lower efficiency. This lower efficiency means that there could be some loss of counts, and since the uncertainty on a peak area follows Poisson statistics thus a higher relative uncertainty in the amount of aluminum in a sample. Since the resolution of the HPGe detector is much narrower than that of both the $LaBr_3$(Ce) and NaI(Tl) detectors, peaks that would normally be merged together are now resolved and clearly visible. This can be both a good and bad thing as if the peaks come from a single escape peak of the element under investigation, then they need to be taken into account, this also means in theory more information can be extracted from the spectra, leading to a better detector response. A disadvantage of semiconductor detectors is that they also need to be cooled either electronically or using liquid nitrogen.

Since detectors need to be operated at sufficiently high voltages (+5000V) in order to maintain drift velocity and full depletion (and therefore efficiently collect electrons and holes), there arises the problem of leakage current. This leakage current is due to the finite conductivity of the detector material. This can be compensated for by properly insulating the detector.

A surface dead layer is created by the thickness of both the p and n contacts, as they will not be infinitesimal. These layers can be up to a few hundred microns thick, which can cause low energy (less than 200 keV) photons to be attenuated before being detected. Obviously, if the layers are too large this can affect the efficiency of the detector at low energies [10,11].

Chapter 2: Methods and Materials

2.1 Phantom Composition

Per [1,2], phantoms were made to contain 14.9 g Ca, 1.29 g Na, 1.19 g Cl, and 220 mg Mg, making them equivalent to concentrations found in the human body, with Al being added in concentrations of 0,250,500,750,1000,2000,5000,10000,50000 micro grams. The phantoms were made by combining nitrate salts (purchased from Milliepore-Sigma) of Ca, Na, Mg with an ammonium salt of Cl with a solution of Al nitrate in nitric acid. The nitrate and ammonium salts were dissolved in water, with the aluminum in nitric acid solution being added last. Using the solubility of each salt the minimum amount of water was calculated to dissolve each salt in water. After the desired amount of each element was added the phantoms were then topped off with distilled water to a total volume of 250 mL. The phantoms were created in duplicate to allow for multiple measurements of each concentration. Efforts were made to keep the amount of each element the same in each phantom, however there were still some minor discrepancies between different phantoms (refer to Tables A1 and A2 for exact amounts, Table 2.1 below summarizes the salts present).

Table 2.1: Salts used for each element in a human hand approximate phantoms and their masses

Element	Salt/Solution	Mass of Salt (g)	Mass of Element (g)
Calcium	$Ca(NO_3)_2 \cdot 4H_2O$	87.8	14.9
Magnesium	$Mg(NO_3)_2 \cdot 6H_2O$	2.32	1.29
Sodium	$NaNO_3$	4.63	1.19
Chlorine	$ClNH_4$	1.8	0.220
Aluminum	Al $(NO_3)_3$ in HNO_3	Dependent on concentration of Al Example: for 5mg Al, use 5mL solution	Dependent on concentration of Al

Elemental phantoms were also produced in duplicate in order to obtain significantly larger amounts than physiologically found and were used in order to calibrate detectors. The Ca elemental phantom was an exception as the amount of Ca was already large enough to produce distinct peaks. For both Mg and Na, this was 10 times the physiological amount, Cl twice, and for Al 0.05g were used. These were to be used in a spectral-decomposition algorithm which used the library data from each element plus a background to fit the spectrum as in [2]

2.2 Irradiation of Phantoms

Each phantom was placed in the irradiation cavity of the Tandem Accelerator (Tandetron) at the McMaster Accelerator Lab (MAL). Protons were accelerated to an energy of 2.3 MeV with a beam current of 400 μA. These parameters were chosen to achieve the optimal neutron fluence rate and have energies that would activate the Al present but not the P and Si present (and therefore avoid contamination from P and Si) in either the phantoms or human body, and to minimize the does to the patients hand during the irradiation. The phantoms were then irradiated for 45s, removed and counted for 10 1 minute cycles in the $LaBr_3$(Ce), HPGe and 4π systems. 10 minutes was chosen as it allows for significant decay of the ^{28}Al isotope (approximately 4 half-lives) allowing .

2.3 Initial Phantom Measurements

For initial results, in order to test if the detectors could detect the Al at all, old phantoms from [1] were used with 5000 μg concentration of aluminum. Average transfer times for these phantoms was 20s from irradiation chamber to detector.

2.4 Al contamination of Bottles and Secondary Phantom Measurements

Unlike with the initial measurements to test if the systems worked, for the next set of measurements Al contamination was a concern. The bottles had no stated concentration of Al present, however it was found in [1] that even the LDPE (low density polyethylene) bottles contained detectable amounts of aluminum. In order to avoid Al contamination after each irradiation the solution was transferred to an un-irradiated bottle and then counted for both HDPE and LDPE bottle types. Average transfer time for the phantoms, accounting for liquid transfer, was 38.4s with a median time of 37.5s.

2.5 Detector Properties

2.5.1 Lanthanum Bromide

The lanthanum bromide detector used is a 2x2 inch cylindrical crystal, with a measured peak resolution of 2.6% at 662 keV (17.2 keV at 662 keV). The power supply used is a Hamamatsu power supply.

2.5.2 NaI(Tl)

The 4π detector array consists of 9 NaI(Tl) detectors arranged in a matrix, with a master control unit attached to all detectors. Anti-coincidence counts were taken in order to suppress the 1.642 and 2.017 MeV ^{38}Cl gammas.

2.5.3 HPGe

The HPGe used is a Canberra Model GC3020, with built in Pre-Amplifier, Model 2002CSL. The detector is a closed-end coaxial with diameter 58mm and length 53 mm, placed 5 mm from the window of the detector. The Dewar has a capacity of 30L. A bias voltage of +5000V was applied

across the signal using the HV power supply from the EG & G Ortec 92x Spectrum Master Spectrometer. The depletion voltage was 4700 V. resolution as stated by the manufacturer was 2 keV (FWHM) at 1.33 MeV, calculated resolution was 1.8 keV at 1332 keV. The stated manufacturer's relative efficiency was 30%, which corresponds to 6% intrinsic efficiency [30]

2.6 Optimization of Lanthanum Bromide Detector

With the initial measurements of the Lanthanum Bromide detector two features were noticed, one was a large spike in the low-energy region of the detector not present in the HPGe or 4π systems, and a lack of energies above approximately 2.5 MeV.

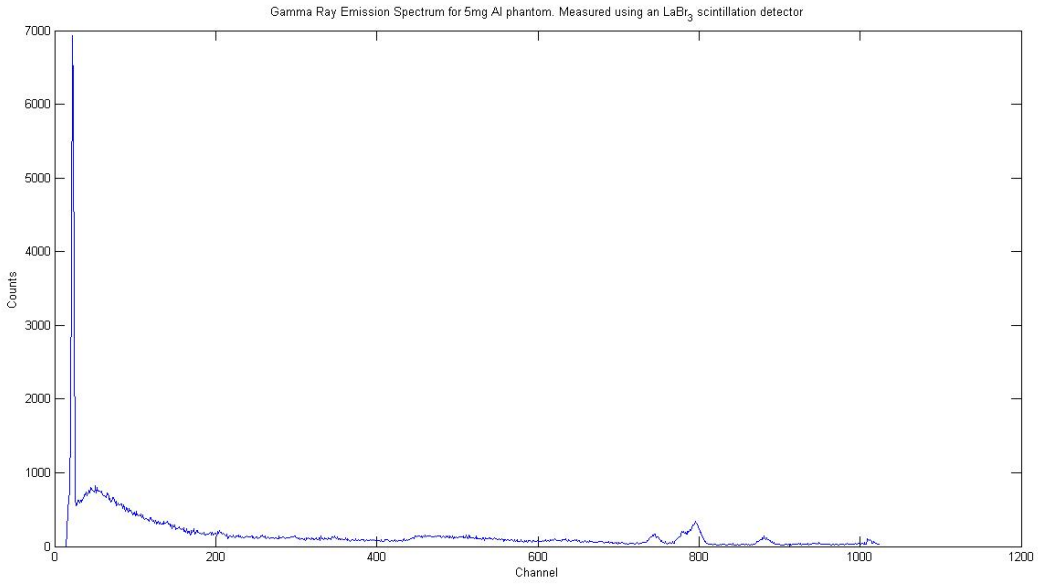

Figure 2.1: Gamma Ray Spectrum for 5000 μg Al phantom, LaBr3(Ce) detector. The large spike in the low-energy region is caused by La X-rays.

In order to investigate the low-energy region a variable x-ray source was used. From here it was found that the x-rays produced corresponded to La x-rays, a result of photons from the Tandetron interacting with the La present in the detector, causing x-rays to be produced. In order to combat

this, the detector was shielded in Pb, as seen in Figure 2.4. The Pb was suspended around the detector using a custom Al framework made by Justin Bennett.

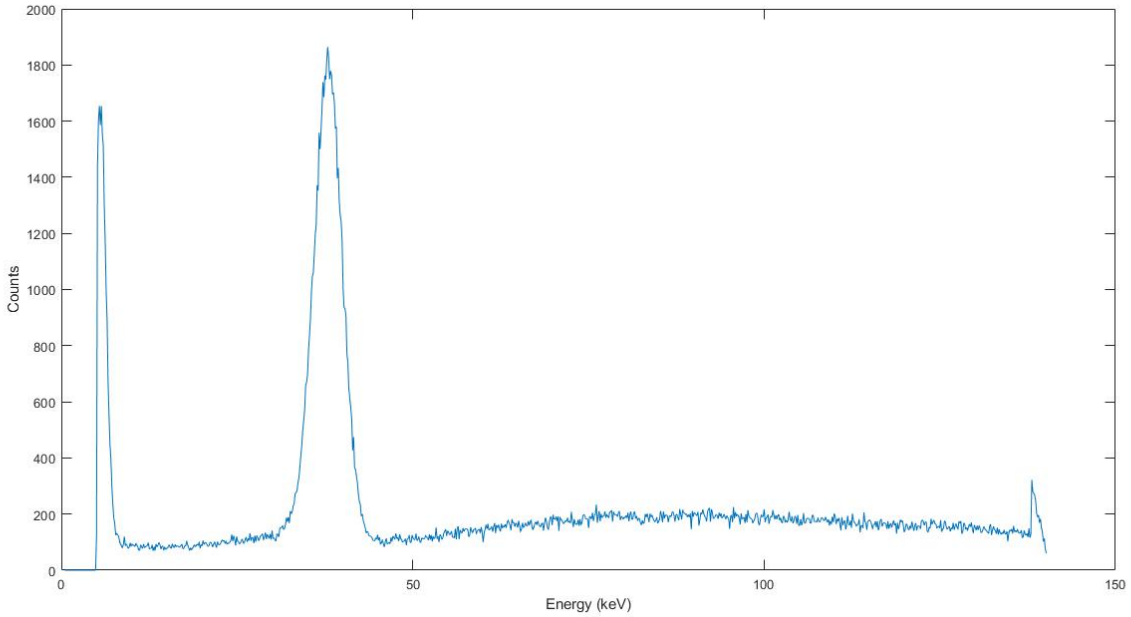

Figure 2.2: La X-rays from the LaBr3(Ce) detector

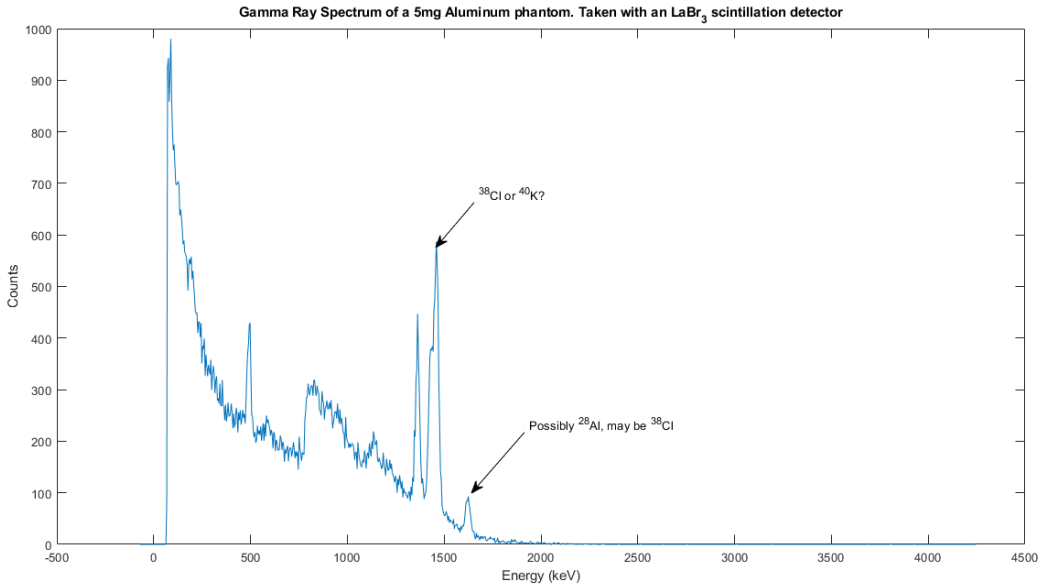

Figure 2.3: Initial Spectrum of LaBr3(Ce) detector. Note the cut-off above 2 MeV

Figure 2.4: $LaBr_3$(Ce) detector setup

In order to investigate the higher energies on the lanthanum, before committing to a full aluminum spectrum. NaCl was irradiated using the Pu-Be alpha-neutron source (McMaster university). Approximately 100g of NaCl was placed in a bottle, then placed into the Pu-Be source and irradiated for approximately 18 to 20 hours, resulting in an approximate activity of 0.895 MBq. The activity of the source was determined by using the equation

$$A = \frac{N_A m \varphi \theta \sigma}{M}\left(1 - e^{-\lambda t}\right) \quad (1)$$

The fluence rate φ is assumed to be $2\text{x}10^6$ [neutrons/s]$\cdot \frac{1}{10\ cm^2} 4\pi = 2.513\text{x}10^6$ neutrons/s cm^2, t=20h, M = 23 g/mol σ = 0.577 b, θ = 1,$N_A = 6.022\text{x}10^{23}$ atoms/mol, m = 39g. The source was then allowed to decay while shielded for approximately 2 hours this was done so that both ^{28}Al (2.25 minutes) and ^{38}Cl (37 minutes) could decay and all that would be left was ^{24}Na. ^{24}Na has

two visible gamma ray energies, one at 1.37 MeV and the other at 2.75 MeV. We are only interested in the higher energy gamma ray as this will help to investigate how the resolution depends on voltage at high energies in the lanthanum.

At a voltage of 700V and gain of 16.69, and resistor feedback pre-amp, the 2.75 MeV gamma ray from ^{24}Na was at channel 575, resulting in a range of energies up to 5 MeV for the $LaBr_3(Ce)$.

2.7 Optimization of HPGe

For the HPGe the conversion gain was chosen such that the peaks would have a relatively wide energy spread, as previous attempts to fit the peaks resulted in very narrow peaks that caused errors when fitting. To do this the number of channels was looked at within the peak, the optimal value was found to be a conversion gain of 35 and 8192 channels.

2.8 Calibration of NaI(Tl)

An in-house auto-gain calibration system was implemented by Kenrick Chin for the 4π system. This greatly increases the speed at which experiments can be performed as the gain voltage for each of the 9 detectors does not have to be inputted manually. Another advantage is this corrects for any gain drift easily. There are however a few issues with the detectors. In order to collect adequate data to calibrate, the system was allowed to collect for approximately a minute. This was done as the detector located at the back of the system is farther away from the source.

The detector was calibrated using a ^{60}Co source. The source was placed in the detector cavity, and a spectrum was collected continuously. While the spectrum was collected a graph of the two ^{60}Co was shown and the second ^{60}Co peak (1332 keV) was calibrated to be at approximately channel 525 on all detectors.

2.9 Peak Fitting

2.9.1 Initial Peak Fitting using nlslm in R

For the initial peak fitting a non-linear least squares Levenberg-Marquardt fitting was performed using the nlslm function in R was used. The basic shape of the peak was modelled as a Gaussian, with amplitude A, mean μ and width σ.

$$F(x) = Ae^{-\frac{(x-\mu)^2}{\sigma^2}} \quad (2)$$

One of the bigger issues with R was its seeming under estimation of the uncertainties. When comparing the results of the uncertainties with a known working FORTRAN code, R's code had the uncertainties be about half of the uncertainties of the FORTRAN results The code was looked at in-depth to try to determine how R was calculating the uncertainties, however this proved fruitless as when the un-transformed uncertainty values were used, they were still half the value of what they should have been. Therefore, it was decided from then on that a previously created FORTRAN fitting algorithm would be used.

Another issue encountered was R would have issues if a channel had no counts in it (i.e. a zero-value). This was of particular issue with the Germanium detector, as the germanium has a very high resolution, but lower efficiency and not as many counts will be registered in each channel as in the lanthanum or sodium iodide crystals, which have a higher intrinsic efficiency. This may have been an issue within R itself as depending on how the chi-square is calculated a divide by zero may occur causing the fit to not work.

The FORTRAN algorithm utilizes non-linear least squares fitting using the Levenberg-Marquardt algorithm. The desired function, initial parameter estimates, and any restrictions on

said parameters are input in the beginning and the code is run. After this, if the values converge, it produces the fitted values of the data along with the chi-square, number of iterations, and parameter estimates along with their uncertainties. From here these values are plotted on a graph to visually check the fit, and the chi-square per channel is calculated to see if there are any channels that need to be excluded or if the model needs to be changed slightly to account for an unforeseen feature in the data.

$$F(x) = C_1 e^{-\frac{(x-C_2)^2}{{C_3}^2}} + C_4 e^{-\frac{(x-C_5)^2}{{C_6}^2}} + C_7 x + C_8 \quad (3)$$

For the NaI(Tl) detector the Al/Cl peak was modelled as the sum of two Gaussians, plus a linear background (see Equation 2), the Ca peak was modelled as a single Gaussian on a linear background. From here the areas for each of the Al and Ca peaks are calculated and are used to calculate the Al/Ca ratios.

Low concentration phantoms were analyzed and the average values for the width and position of the Al peak were calculated. These values were 348.27 for the position and 13.5462 for the width respectively. These values then transformed equation (2) into the following:

$$F(x) = C_1 e^{-\frac{(x-C_2)^2}{{C_3}^2}} + C_4 e^{-\frac{(x-348.27)^2}{13.5462^2}} + C_5 x + C_6 \ (4)$$

2.10 Data Collection HPGe and Lanthanum Bromide

MAESTRO was used to collect all spectra for the HPGe and $LaBr_3$, with a custom looping code in order to collect 10 1 minute cycles.

2.11 Miner Selection

Miners were invited to participate in the study via the McIntyre Powder Projects founder Janice Martell. Participation was voluntary and the miners could drop out at any point for any reason. Once selected each miner's working history was assessed and placed in one of three categories: low, medium and high exposure. From here 5 miners from each category (for a total of 15) were chosen at random and invited to the McMaster Accelerator Laboratory for irradiation.

Each participant was given a study number (001 – 015), and was assessed by Dr. David Cowan. Cognitive tests performed were as follows: MOCA test, Trail-making Test Part B (TMT-B) and the Digit Symbol Substitution Test (DSST). [32]

DSST measures mental speed, attention and frontal-executive function. MOCA is used for a broad range of disorders including Alzheimer's, Parkinson's and stroke. It is able to identify more subtle cognitive deficiencies. TMT-B measures frontal-executive function.

2.12 McIntyre Powder Project Participants

For the irradiation participants were brought in, fitted with a water sleeve to prevent excess neutron radiation from escaping the chamber which would increase torso dose, and were irradiated for 45s at 400 μA, 2.3 MeV. A caregiver was present with them during the procedure to facilitate ease of transport. After the irradiation the water sleeve was drained, and the participant was moved to the 4π (either via wheel chair or walking). Average transfer time was 57.3s and median transfer time was 58.8s. After that the participants irradiated arm was counted for 10 cycles of 1 minute each. There were two instances where things went wrong with the counting. For one participant after an option on the counting software had been selected, the detector stopped counting after the first cycle. This was not found until approximately 5 to 6

minutes after. The count was re-done after this (P003). The other issue was one patient had their wrong arm placed in the 4π, this was noticed after approximately 1 minute after which their correct arm was placed in the 4π and counted. Dose to the patient's hand was assumed to be 2.5 mR, the same as in [1]. A correction factor was applied using the decay formula $N = N_0 e^{-\lambda t}$, where t is the time difference between the start of counting for the calibration phantoms, and the start of counting for the miners.

2.13 Calculation of MDL

The MDL was found by taking 2 times the average uncertainty in the lower concentration phantoms and dividing by the slope of the calibration line.

2.14 Peak Analysis

For both the Germanium and Lanthanum detectors the LM fitting algorithm unfortunately was not able to work. So an alternative approach was implemented.

As the germanium spectra's peaks were quite small, the first 3 cycles were summed together before fitting. From here the start and end-points of the peak were determined and the counts under the peak were summed. From here a linear background was estimated and then subtracted off. Errors were calculated following standard error analysis practices.

For the lanthanum fits a different, but similar method was employed. Instead of summing the first 3 cycles the first 3 cycles were looked at individually. For these, similar to for the germanium runs, the start and end-points of the background were determined, and the counts were summed for the peak. After this a set number of channels (i.e. 4) were taken on either side of the peak to be the low and high-end background counts. These counts were averaged and any difference in number of channels was taken into account by multiplying by the number of

channels in the peak and dividing by the number of channels in the background. The resulting counts were then subtracted off the peak counts, resulting in the net area of the peak.

This process was repeated for each cycle, and concentration. From here the slopes were calculated and the MDL was found by taking the average of the low concentration uncertainties, then taking the inverse-variance weighted mean and dividing by the slope in order to find the MDL in μgAl.

2.15 Calculation of Solid Angle

The sources (irradiated phantoms) used are cylindrical Nalgene bottles, and will thus be modelled as a cylindrical source. The distribution of the radiation throughout the volume is assumed to be constant in order to simplify calculations. In order to calculate the average solid angle for the source, a few approximations were made. Along the axial direction of the detector (z-axis), as one moves away from the point source towards the detector the solid angle becomes larger as more radiation will be able to hit the detector window, as one moves further away from the detector face the solid angle becomes smaller. Thus, on average, along the axial direction the solid angle will be that of a point source, meaning this does not need to be modelled. For the (x,y) plane as you move further away from the point-source in either direction the solid angle on average will decrease. The average is taken by taking the integral of the solid angle of the point source over a volume, then dividing by a volume. In order to solve this, it must be done analytically.

The solid angle for each circle depends on the angle, the radius and the distance from the centre of the cylinder to the source. In order to calculate geometry was used, and certain

approximations were used such as the distance between the side of the source and the detector being approximately zero.

The integral of the source was approximated as a series of discs. Following the procedure outlined in [14] the equation for a detector located in the X-Y plane, shifted by distance ρ, and a source in the X-Z plane shifted by height h_o is given as: [14]

$$\Omega = 2\pi - \frac{4}{\pi(R_s)^2}\int_0^{R_s} dqq \int_0^{\pi} d\psi h \int_0^{\pi} d\varphi \frac{h^2+\rho^2+R_d\cos(\varphi)}{h^2+\rho^2-\rho^2 cos^2(\varphi)} * (h^2 + \rho^2 + R_d + 2R_d\rho\cos(\varphi))^{-\frac{1}{2}} \quad (5)$$

$$h = Z \quad (6)$$

$$\rho = [(\rho_o - X)^2 + Y^2]^{-\frac{1}{2}} \quad (7)$$

$$X = x'\cos(\alpha) \quad (8a)$$

$$Y = y' \quad (8b)$$

$$Z = x'\sin(\alpha) + h_o \quad (8c)$$

$$x' = qcos\psi \quad (9a)$$

$$y' = qcos\psi \quad (9b)$$

$$z' = 0 \quad (9c)$$

Where x',y' and z' are the shifted axes, with the origin at the centre of the detector. q is the distance the detector has been shifted and ψ is the angle it has been shifted.

Alpha is the angle from the X-axis which in this case is assumed to be zero. The height, h_o stays constant and is assumed to be the radius of the source, as the source was placed directly in front of the detector face.

The integral was calculated numerically in MATLAB to see if it was similar to the values given in the paper, the value output from MATLAB was 0.0072 [sr] while the paper was 0.007361 [sr].

In order to check that this is correct, the solid angle for a very small radius of the circle is calculated and compared to that of a point source. The point source formula for a cylindrical detector and point-source in 3-D is given by the following equation

$$\Omega = 2\pi\left(1 - \frac{d}{\sqrt{d^2+a^2}}\right) \quad (10)$$

Where a is the radius of the detector and d is the distance from the point source to the detector.

This was tested using the lanthanum bromide detector, the value calculated for the point source was 1.442 [sr] and the value for a small radius was given as 1.445 [sr].

Since the ρ_o values are the shift along the x-axis (i.e. the distance laterally between the source and the detector) in order to find the average source volume solid angle. To do this the value of ρ was changed in small increments (i.e. 0, 0.5, 1 etc) and the solid angle for that ρ was calculated. Each solid angle value was then summed and divided by the volume of the source to get the average solid angle.

.

Chapter 3: The 4π Detector System

3.1 4π System:

In order to be able to tell how much aluminum was present in either a sample or a person, it first needs to be determined how many counts in the system correspond to different concentrations of aluminum. As per sections 2.1 and 2.2, phantoms of varying aluminum concentrations were created in duplicate and irradiated under the same proton current and energy protocol (400μA, and 2.3 MeV respectively). The areas of both the Al and Ca peaks were calculated, again as per section 2.1, and calibration lines were created.

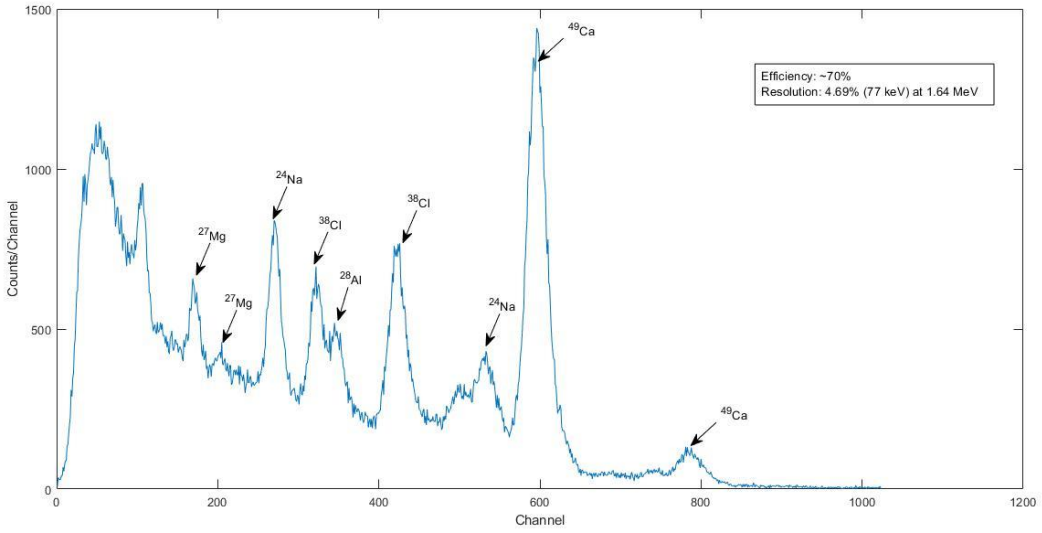

Figure 3.1: Labelled Spectrum for a 2000 μgAl phantom for the 4π NaI(Tl) detector setup

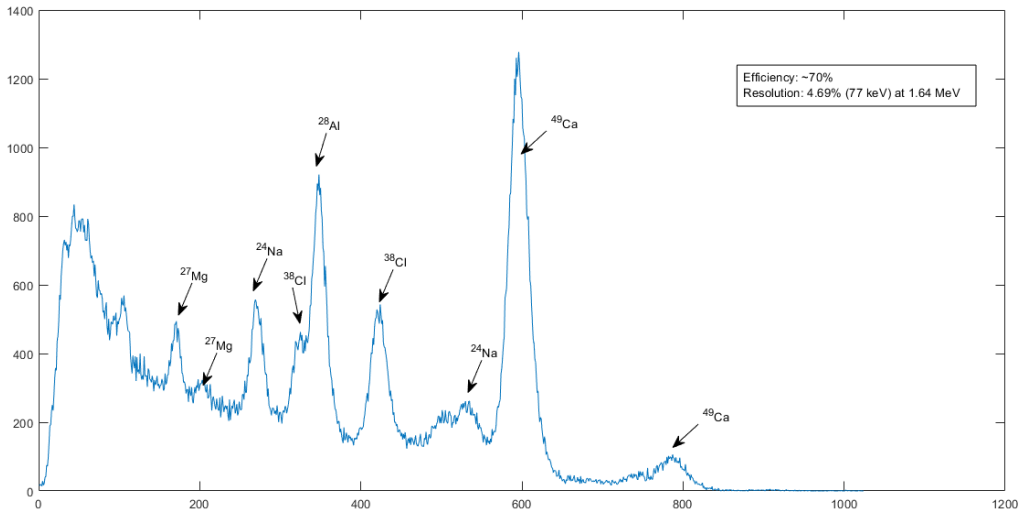

Figure 3.2: Labelled Spectrum for 10000 µgAl phantom

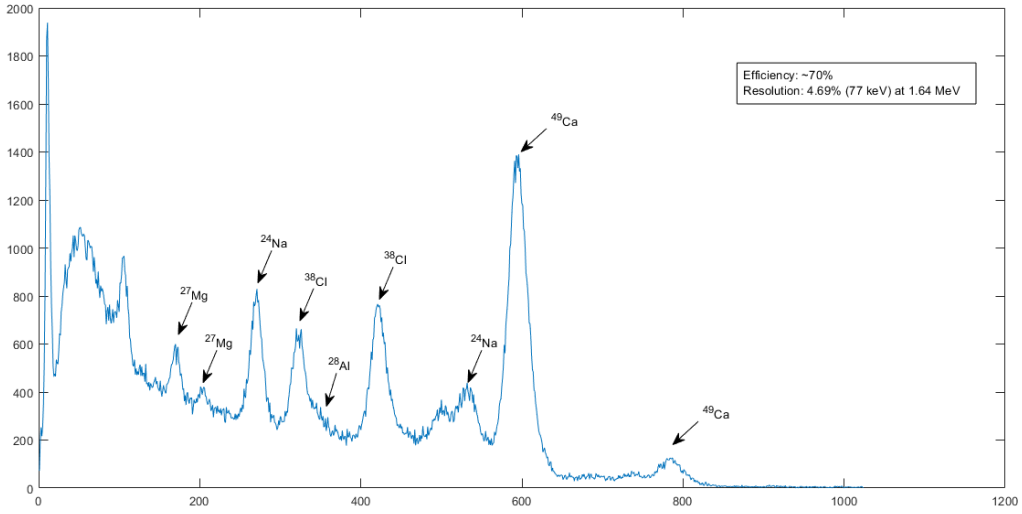

Figure 3.3: Labelled Spectrum for 250 µgAl phantom

Calibration lines were created for the first 180s of counting time, each with a cycle of 60s resulting in three calibration lines. This was done to avoid accidentally overpowering or

obscuring any features present in either the phantoms or in-vivo data. It also means that the decrease in Al/Ca concentration can be looked at as a series of time (if needed).

For each phantom, the Al (1.78 MeV), Cl (1.64 MeV) and Ca (3.08 MeV) photopeaks were fit using a Gaussian on a linear background. The fitting model was determined based on the principal that each peak will be a Gaussian function on a background. The specific model was determined based on previous work by [1], different backgrounds were tried but ultimately the linear background gave the best fit.

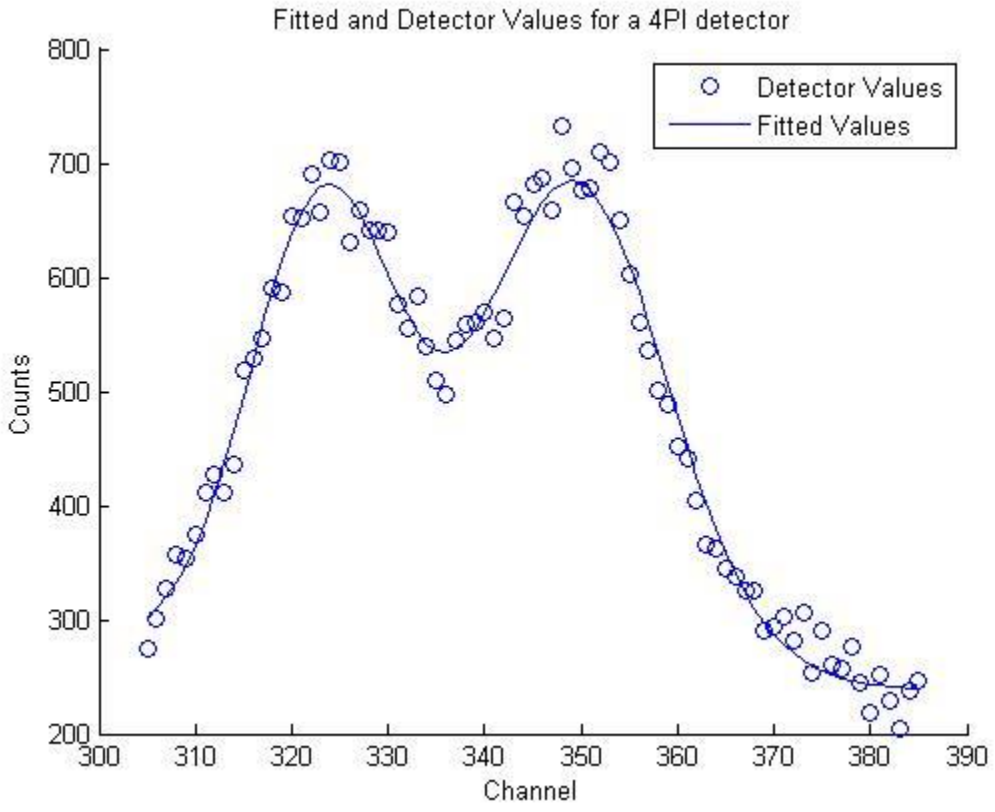

Figure 3.4: Fitted data for Al/Cl peak for 5000 μg Al phantom. The Cl peak is on the right, Al peak on the left. Note how both peaks have significant overlap with each other. $X^2 = 1.2253$

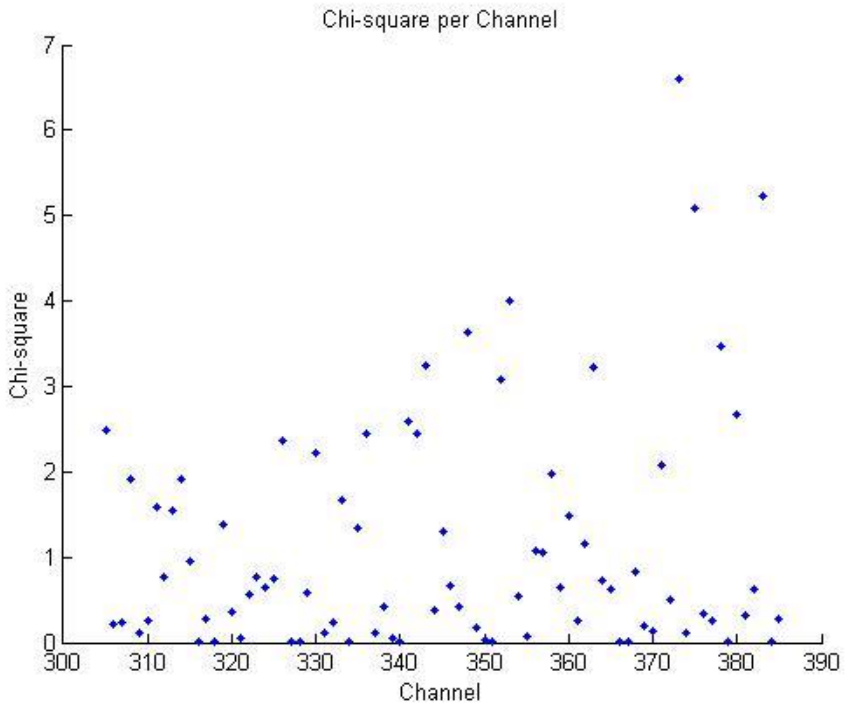

Figure 3.5: Chi-square distribution for Al/Cl fit for a 5000 μg Al phantom

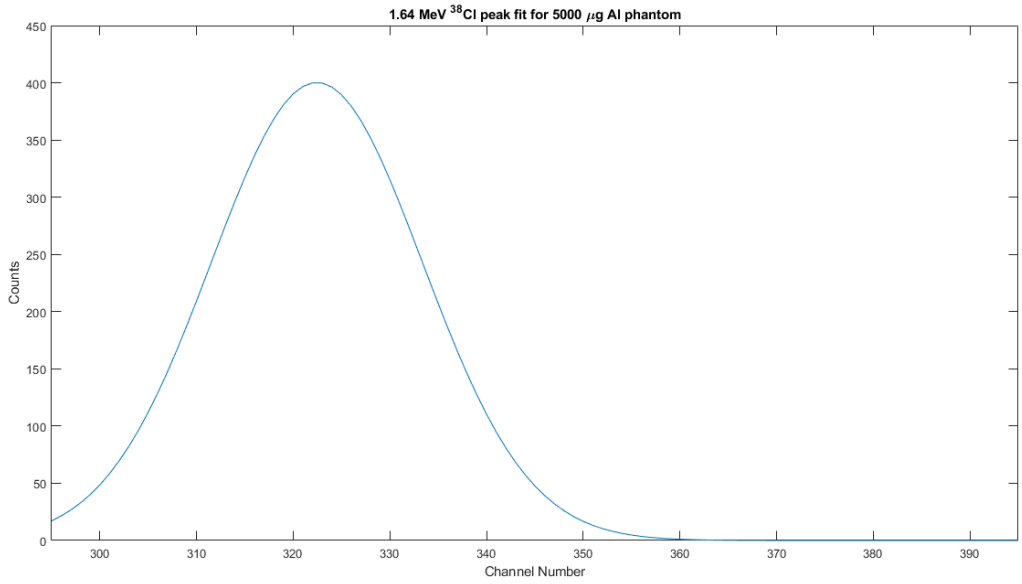

Figure 3.6 Separate fitted peak for the 1.64 MeV peak for a 5000 μg Al phantom

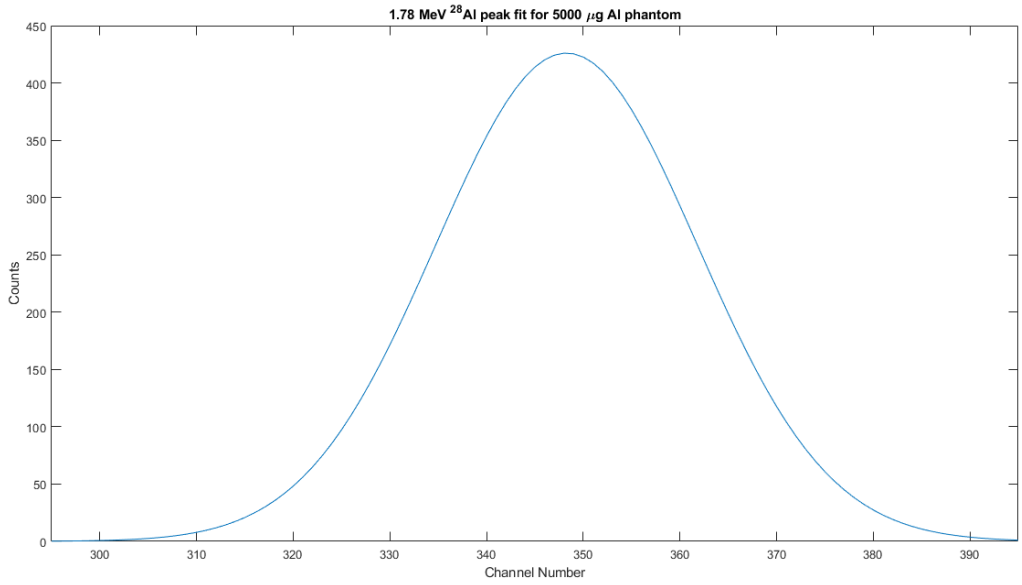

Figure 3.7: Separate fitted peak for the 1.78 MeV peak for a 5000 μg Al phantom

Figures 3.4 and 3.5 show both the fit as well as the chi-square distribution for the Al/Cl combination peak for a tissue equivalent phantom with 5000 μg Al. As can be seen from the chi-square data, there do not appear to be any unseen features affecting the distribution of the chi-square, meaning that further fitting is not needed and values can be used. Though in Figure 3.4 there is a dip that is not properly fitted.

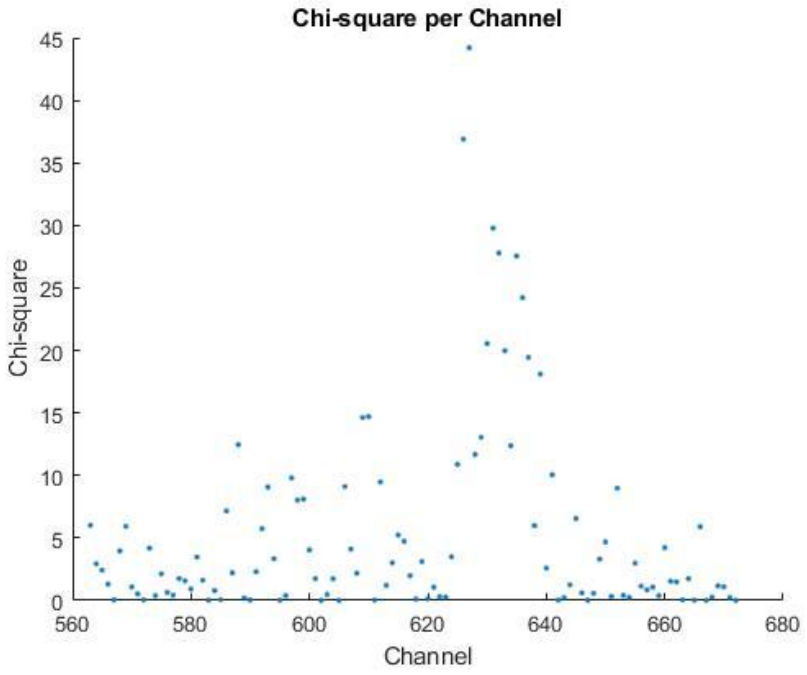

Figure 3.8: Chi-square for Ca fit for 5000 μg Al phantom

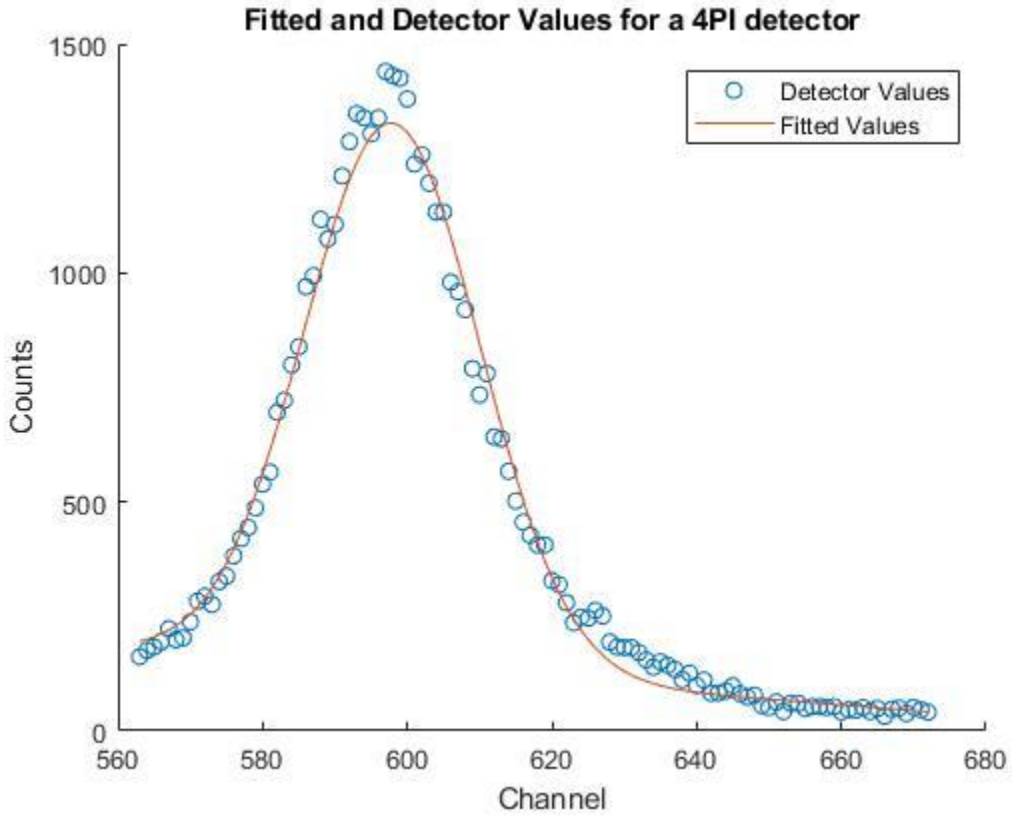

Figure 3.9 Fit for Ca for 5000 μg Al phantom, $X^2 = 4.396$.

As can be seen from Figure 3.6, and 3.7, for the Ca peak the right hand tail is severely underestimated. This may have been due to detector gain shift over time, however it was found that this undershoot did not significantly affect the area of the peak, so this feature was ignored. For a number of phantoms, the number of channels for the Ca peak was reduced on the right hand side in order to help decrease the chi-square.

In order to see if the shift was present in the lower energy region the lower energy 24Na peak was fitted using the same Levenberg-Marquardt algorithm for the 5000 ug phantom to compare. As can be seen from Figures 3.10 and 3.11 below, the undershoot/shift in the lower energy region is not present compared to the higher energy region. Meaning that this shift is only of great concern in the higher energy regions of the detector.

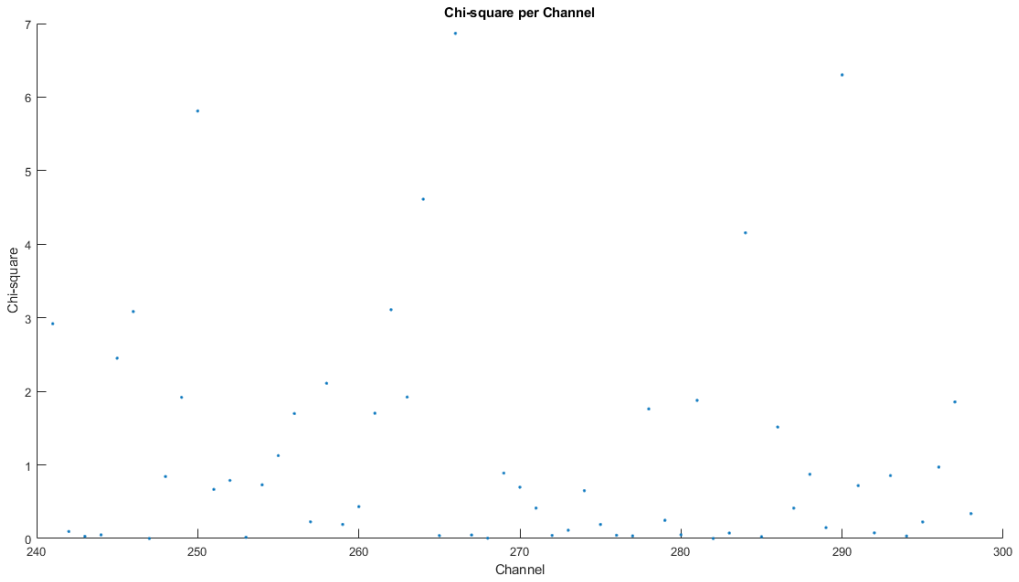

Figure 3.10 Chi-square distribution for ^{24}Na peak for first 60s cycle for a 5000 μg Al phantom

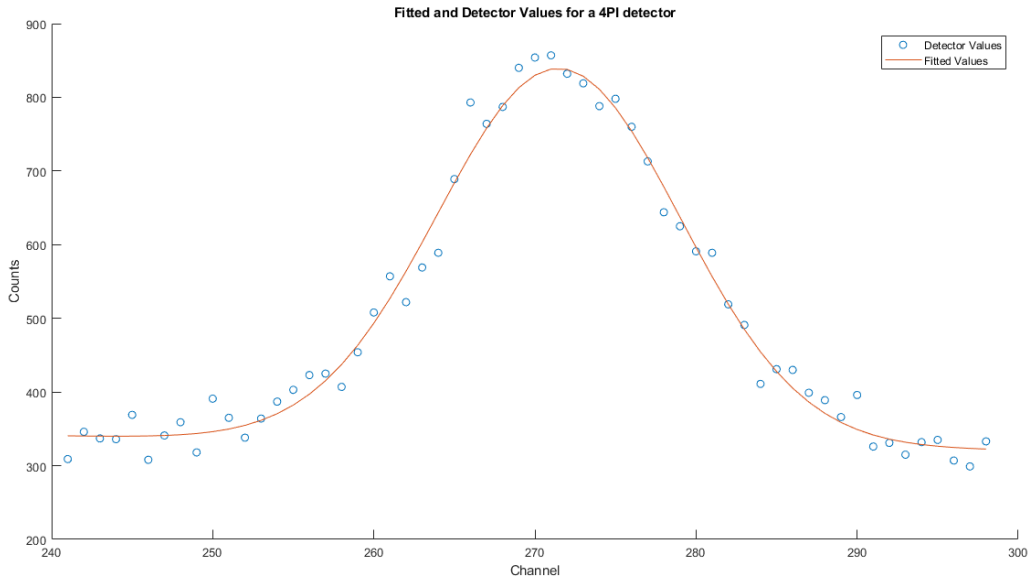

Figure 3.11 1.37 MeV peak of ^{24}Na for first 60s cycle for a 5000 μg Al phantom, X^2 = 2.3545

Table 3.1: Cycle 1 Values NaI(Tl)

Phantom	Al Area	Ca Area	Al/Ca
0_1	16079.53±1260.17	45869.29±493.80	0.3506±0.0277
0_2	1165.35±454.26	54430.58±545.62	0.0214±0.0083
250_1	2177.01±242.09	44206.17±457.16	0.0492±0.0055
250_2	2458.40±278.03	53059.91±498.66	0.0463±0.0046
500_1	4248.83±381.07	60142.38±528.52	0.0706±0.0064
500_2	3432.88±332.93	52787.64±511.50	0.0650±0.0065
750_1	6426.38±534.55	57465.08±525.37	0.1118±0.0094
750_2	5333.36±455.06	59636.77±538.46	0.0894±0.0077
1000_1	5962.89±497.56	61221.39±535.07	0.0974±0.0082
1000_2	5433.19±465.23	60385.37±531.26	0.0899±0.0077
2000_1	6081.05±506.18	52238.14±507.88	0.1164±0.098
2000_2	7751.65±622.25	51526.63±505.34	0.1504±0.012
5000_1	10773.14±811.93	59246.64±202.85	0.1818±0.0137
5000_2	14466.65±1104.65	49786.68±496.48	0.2906±0.0224
10000_1	27900.07±488.14	54465.62±551.63	0.5123±0.0104
10000_2	20796.41±416.25	46410.51±524.68	0.4481±0.0103
25000_1	74310.37±811.43	59921.22±577.79	1.2401±0.0181
25000_2	69081.31±711.47	52953.25±555.08	1.3046±0.0192
50000_1	120618.10±945.26	53777.72±557.03	2.2490±0.0291
50000_2	118962.80±965.17	54195.94±576.92	2.1950±0.0294

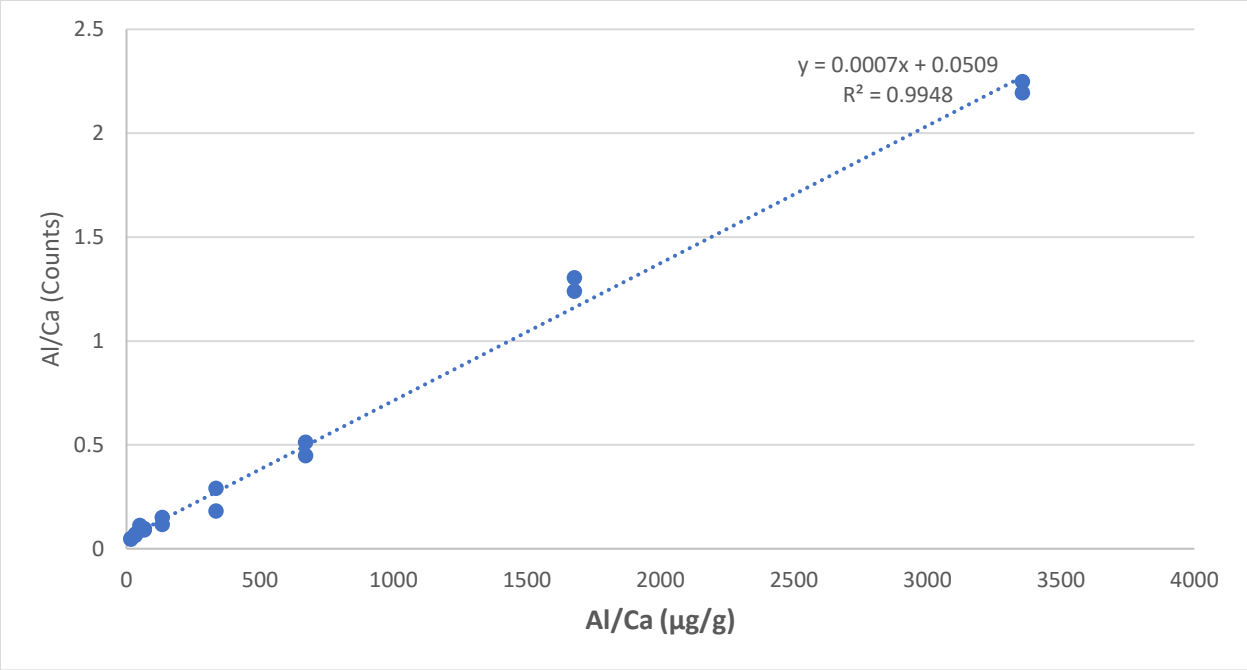

Figure 3.12 Calibration Line T1, for first 60s cycle. Equation calculated using Excel's LINEST function

Table 3.2: Cycle 2 values NaI(Tl)

Phantom	Al Area	Ca Area	Al/Ca
0_1	-752.55±422.98	41689.20±473.24	-0.0181±0.0101
0_2	1314.89±445.20	49726.52±525.63	0.0264±0.0090
250_1	1993.96±239.93	40823.73±443.82	0.0429±0.0056
250_2	1973.52±255.99	46043.65±514.24	0.0488±0.0059
500_1	3473.91±342.01	55046.42±508.84	0.0631±0.0062
500_2	2819.00±301.83	47334.57±525.22	0.0596±0.0064
750_1	5206.36±456.50	54466.37±508.58	0.0956±0.0084
750_2	4467.16±406.62	54906.20±553.64	0.0814±0.0075
1000_1	4527.60±412.00	56636.02±514.45	0.0799±0.0073
1000_2	4822.67±430.48	54780.05±554.98	0.0880±0.0079
2000_1	4550.69±411.76	48167.20±488.16	0.0945±0.0086
2000_2	5731.31±489.50	46515.56±525.95	0.1232±0.0106
5000_1	10519.69±822.32	47450.08±480.05	0.2217±0.0175
5000_2	11754.98±914.29	44642.45±516.69	0.2633±0.0207
10000_1	24297.05±1825.94	50152.60±538.06	0.4845±0.0368
10000_2	17098.19±1293.09	43350.63±507.42	0.3944±0.0302
25000_1	54192.36±714.17	54688.67±554.93	0.9909±0.0165
25000_2	50609.32±647.39	48235.27±533.00	1.0492±0.0177
50000_1	89298.93±834.29	49835.52±530.76	1.7919±0.0254
50000_2	87735.83±848.51	51631.83±554.57	1.6993±0.0246

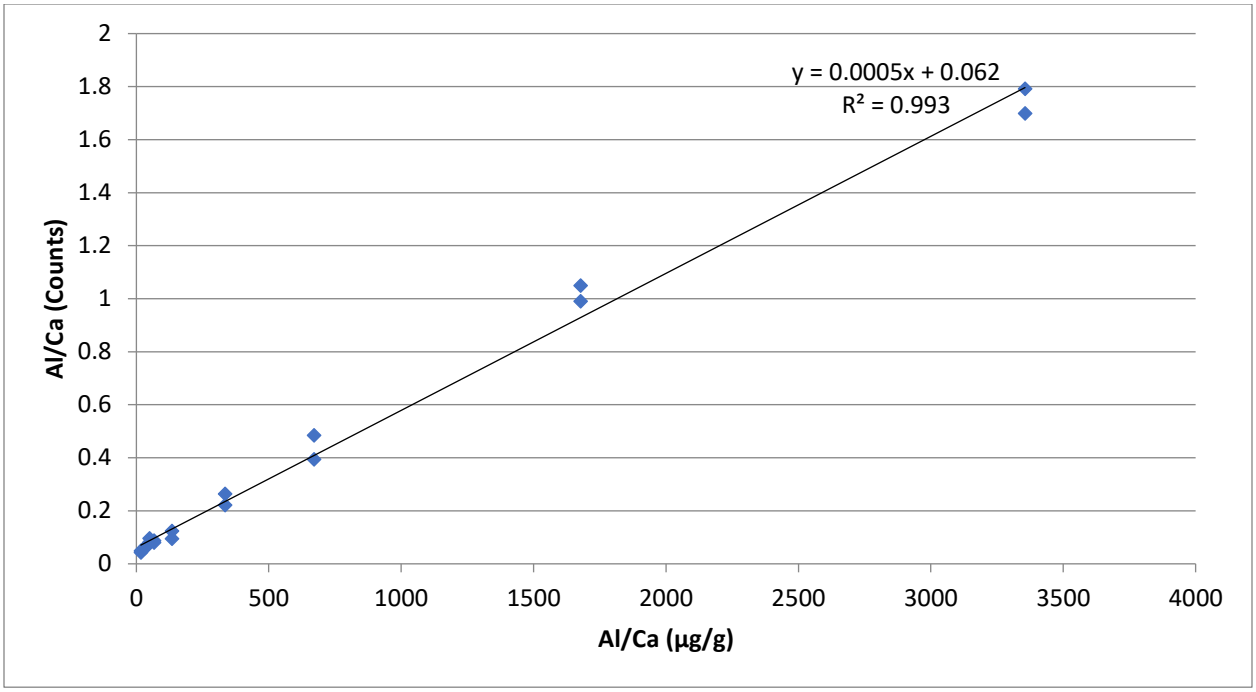

Figure 3.13 Calibration Line T2, for second 60s cycle. Equation calculated using Excel's LINEST function

Table 3.3: Cycle 3 values NaI(Tl)

Phantom	Al Area	Ca Area	Al/Ca
0_1	-2286.21±433.33	38563.55±458.54	-0.0593±0.0113
0_2	2316.33±457.24	45634.73±506.28	0.0508±0.0100
250_1	1256.65±203.09	37053.39±424.16	0.0383±0.0055
250_2	1655.05±237.21	43242.28±494.73	0.0339±0.0055
500_1	3019.86±312.01	51274.37±491.59	0.0589±0.0061
500_2	2250.73±269.24	42869.08±503.11	0.0525±0.0063
750_1	4028.46±378.23	49111.74±484.86	0.0820±0.0077
750_2	3460.72±342.42	50263.56±531.91	0.0689±0.0069
1000_1	3623.03±351.65	52930.43±498.31	0.0684±0.0067
1000_2	3353.59±336.74	50286.98±532.10	0.0667±0.0067
2000_1	3638.31±350.90	44213.04±468.53	0.0823±0.0080
2000_2	4690.58±420.61	42375.92±500.70	0.1107±0.0141
5000_1	7351.66±596.24	42522.00±456.90	0.1729±0.0158
5000_2	8328.55±669.02	42898.11±499.01	0.1941±0.0282
10000_1	17201.75±1306.31	46794.27±511.21	0.3676±0.0245
10000_2	12626.61±965.73	39955.54±488.22	0.3160±0.0154
25000_1	40201.74±660.98	50936.67±536.93	0.7892±0.0159
25000_2	38050.97±577.18	45401.96±513.32	0.8381±0.0159
50000_1	66351.78±729.10	45984.38±516.23	1.4429±0.0227
50000_2	66352.41±767.00	46490.23±530.69	1.4272±0.0232

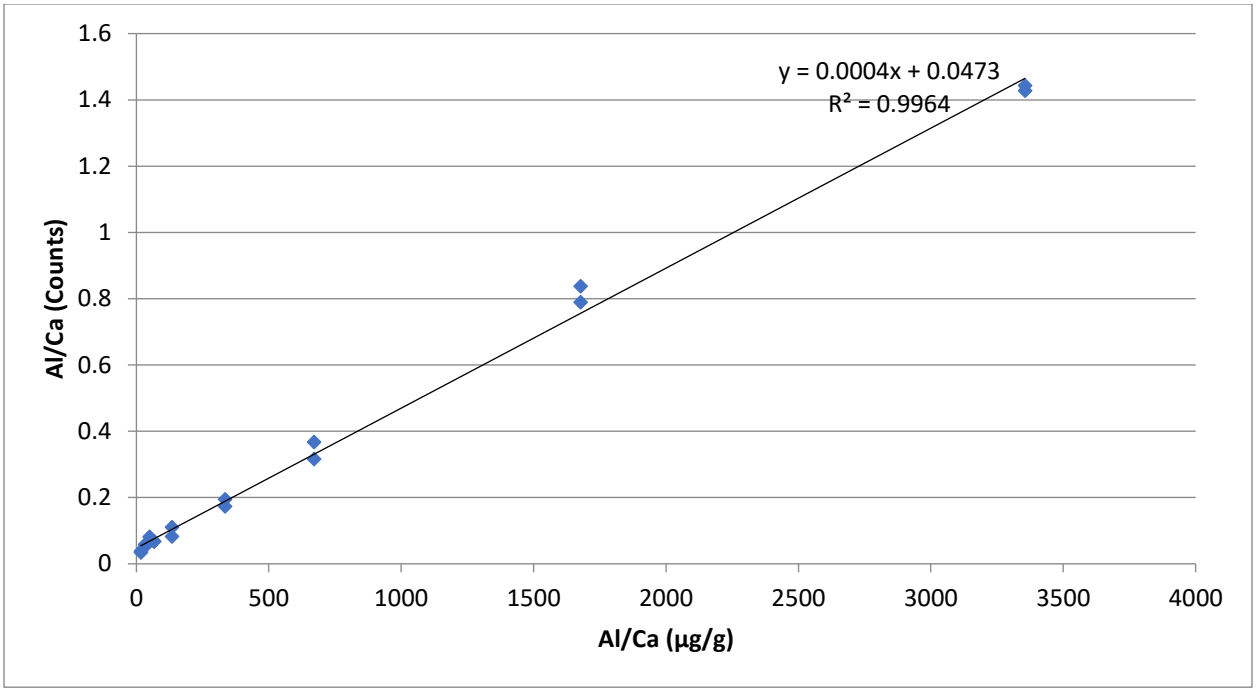

Figure 3.14 Calibration Line T3, for third 60s cycle. Equation calculated using Excel's LINEST function

The MDL of the system was calculated to be 22.57 µgAl/gCa for in-vivo measurements, 3 times bigger than previously calculated for [1]. The MDL for in-vivo measurements was calculated by taking the median uncertainty of all in-vivo measurements and multiplying by 2, as seen in [1. The phantom MDL was calculated as per section 2.13 by taking two times the uncertainty of the zero phantom for each cycle, these were then added using inverse variance weighting, which gave an MDL of 15.85 µgAl/gCa or 236.16 µgAl. Please note that due to the variations in the 0 ug Al phantoms, they were left out of the calibration lines, and thus the MDL calculations.

3.2 Miner Data:

Following the procedures outlined in section 2.2, miner data were analysed via photopeak analysis. While P001 – P003, P005, P007 and P008 were fit using the standard Al, Ca, Cl fits. P009 – P015 presented with another feature at approximately 10 to 20 channels to the right of the

Al (1.78 MeV) channel. This unknown peak was fit with an additional Gaussian. This resulted in an increase in the Al photopeak area, as well as a decrease in the uncertainty of the area.

Energy calibration for each participant's data was done individually based on various identifiable elemental peaks (such as ^{38}Cl, ^{24}Na, etc). This was done to minimize any shift in gain over the course of the irradiation/counting periods. This was then used to transform the number of channels to energy in order to locate peaks.

P009 had the wrong hand in the detector for the first 4 minutes, after this, it was noted and cycles 4 to 6 were analyzed as the first three cycles.

P004 – P015 did not show any abnormal features, so no additional peaks were investigated. Participants 004 and 009-014 all had negative concentrations of Al/Ca, meaning that the amount of aluminum present in the participant was less than the MDL of the system, which varied from participant to participant since the uncertainty varied quite widely for each participant. For participants that were above the MDL, P001 had the highest concentration at 206.36±14.76 μgAl/gCa and P005 had the lowest concentration at 18.55±3.95 μgAl/gCa.

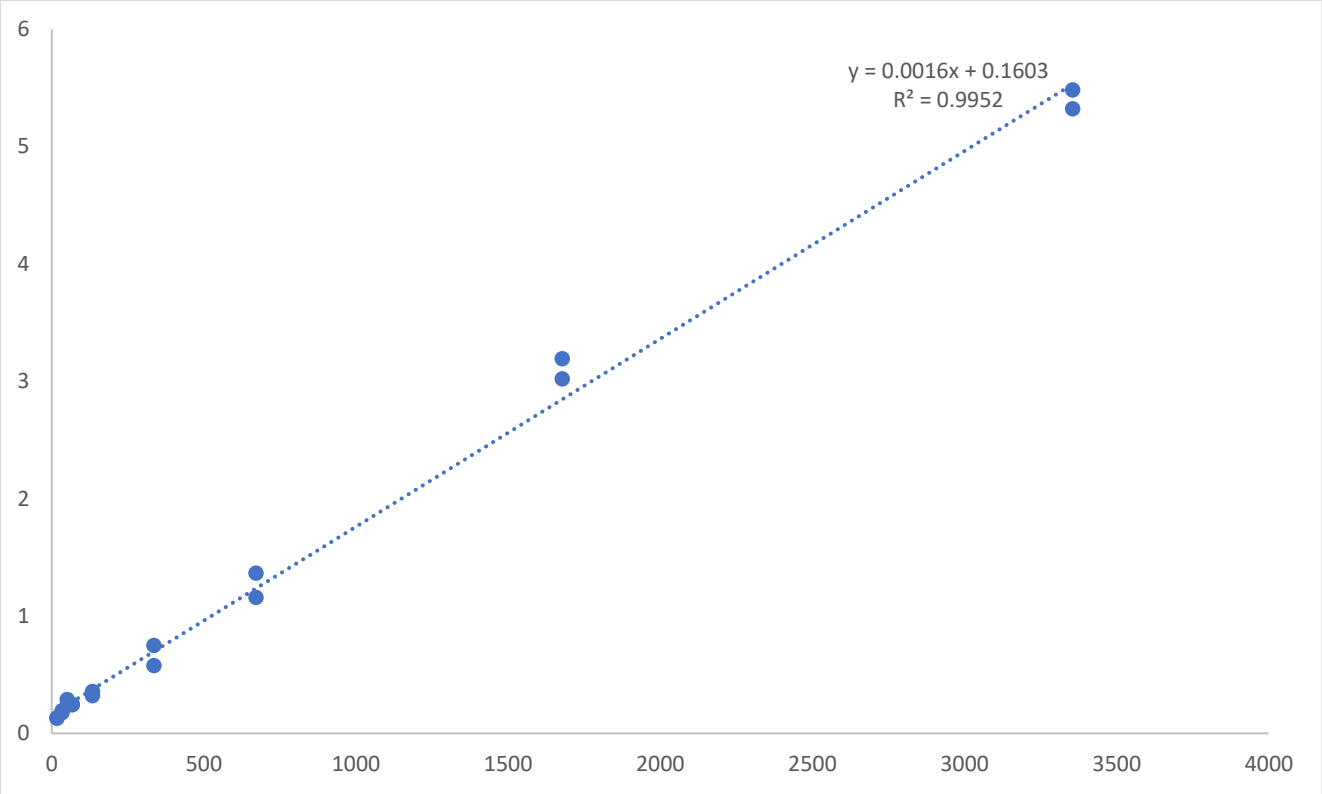

Figure 3.15 Calibration line for first three 60s cycles, instead of utilizing IVWM, the values for each cycle were summed, thus creating this calibration line.

Table 3.4 Concentrations of Al per gram Ca in Miner population.

Participant Number	Al/Ca Concentration (μgAl/gCa) inverse variance weighted	Summed
P001	206.36±14.76	207.87±15.85
P002	31.12±21.96	73.62±27.63
P003	27.80±7.84	12.17±3.43
P004	-34.21±15.20	-34.88±17.14
P005	18.55±3.95	18.42±4.18
P006	44.76±7.77	48.12±9.66
P007	29.48±6.31	28.41±6.58
P008	67.88±9.67	70.93±10.11
P009	-46.08±19.96	-59.26±83.05
P010	-34.71±13.77	-40.64±56.41
P011	-13.41±14.81	-13.02±26.90
P012	-13.80±11.28	-22.79±24.42
P013	-23.89±42.87	-39.31±56.41
P014	-22.23±8.05	-19.15±17.98
P015	23.85±8.48	22.05±8.96

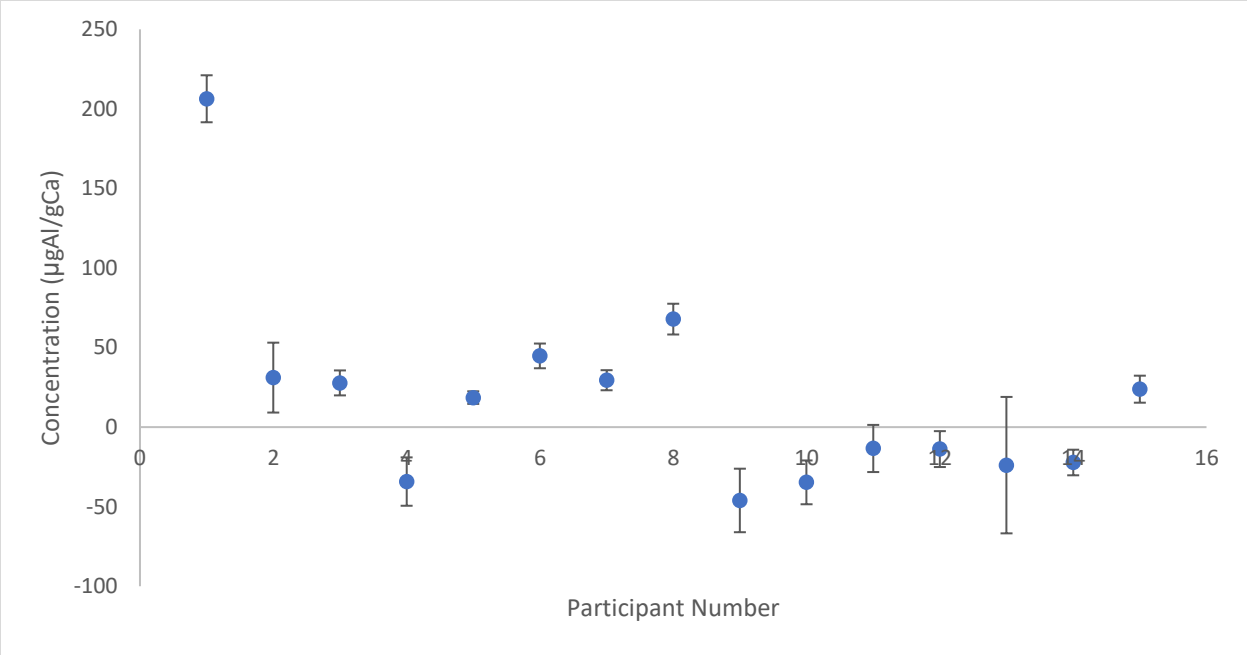

Figure 3.16 Inverse Variance Weighted Miner Concentrations

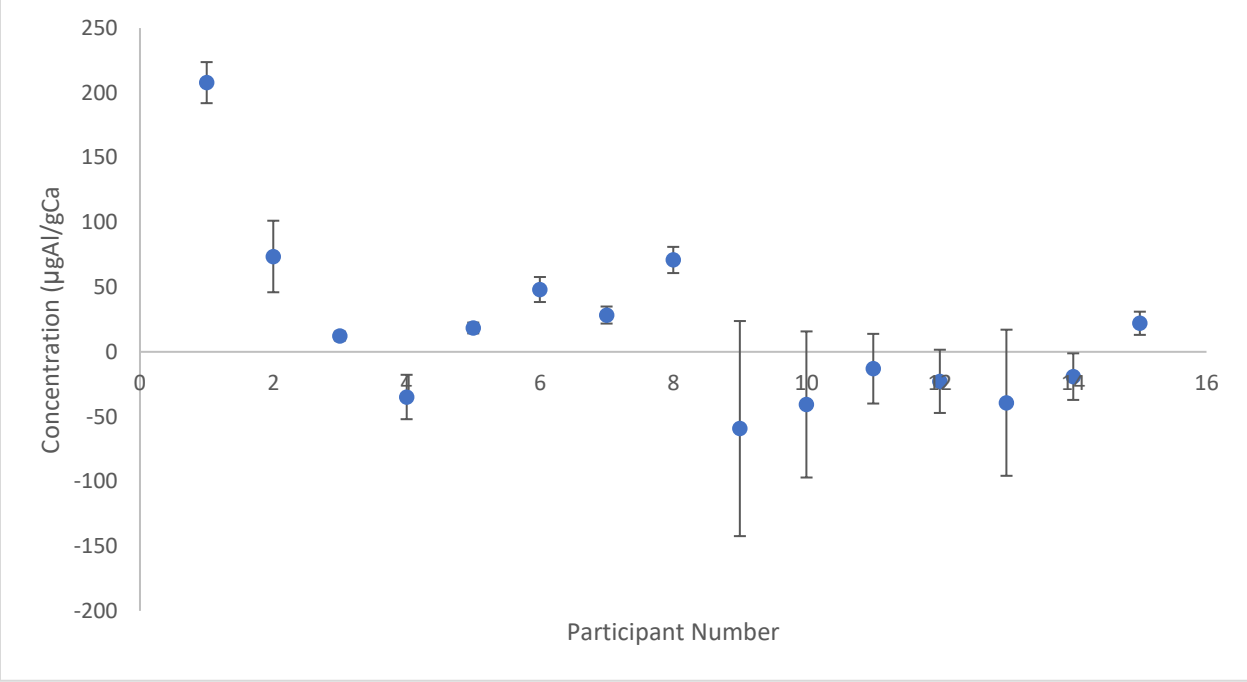

Figure 3.17 Summed Miner Concentrations

Figure 3.16 show the distribution of the concentrations of Al in bone for all 15 patients. As can be seen participant 001 had the highest concentration significantly higher than the other 14 participants. At the time of analysis occupational information on participants was not available, though given the amount it is likely that this individual was exposed to a much higher amount of Al compared to their peers.

Differences in uncertainty ranges are most likely due to counting statistics and the variation of concentrations of each element in each person, which leads to differing activities of each element and therefore different uncertainties. Another contributing factor may also be the error in the fitting of the model itself, as with lower concentrations (smaller peaks) the algorithm cannot determine the characteristics of the peak as accurately as with higher concentrations (larger peaks).

The in-vivo MDL was calculated via IVWM, with a value of 22.57 μgAl/gCa. In order to see if there would be any significant difference the MDL using the sum of the first three cycles was calculated instead of the IVWM.

For the sum of the first 3 cycles the MDL was found to be 34.29 μgAl/gCa for the in-vivo measurements. The mean calculated values for both, however, are within error of each other suggesting that while the errors may be grossly underestimated the data are not.

The IVWM was also much more precise than the summed mean. Due to the IVWM having lower errors, and therefore being more precise this is the one we will go with.

The mean of the differences between the summed and IVWM was -0.329±26.454 μgAl/gCa.

3.2.1 Special Cases:

For patients 001 to 003 there were some interesting features. Patient 003 unfortunately had an error occur with their data collection, the software failed to record past the first initial cycle, which was not noticed until about 5 minutes later, a subsequent 10 minute count was performed after this error was noticed. Fortunately, there was still the initial 60s cycle immediately following irradiation.

P001 presented with a large peak just before the first Na peak at 1368 keV. The peak was fit with a single Gaussian, and the areas were calculated for cycle 1 and cycle 10. From these areas the half life was calculated using the radioactive decay formula. The half-life was found to be 2.552±0.796 h, with the energy being 843 keV, which is within error of the half-life for the isotope ^{56}Mn, which has a half-life of 2.5785 h, with a gamma emitted at 98.9% of the time at 846.771 keV. Mn is naturally found in trace quantities in the human body, assisting in enzyme function, so its presence is not in and of itself a surprise [15]. Mn is also found in welding fumes, and has shown to be associated with neurological conditions [29] What is a surprise however is how large the peak is, as the peak has an area twice that of the 3.08 MeV Ca peak, suggesting that there is a large amount of Mn present in the skeleton of the individual.

Time	Unknown Area	Unknown Area Error
T1	39101	449
T10	37539	421

Table 3.5 Unknown Peak Area for participant P001

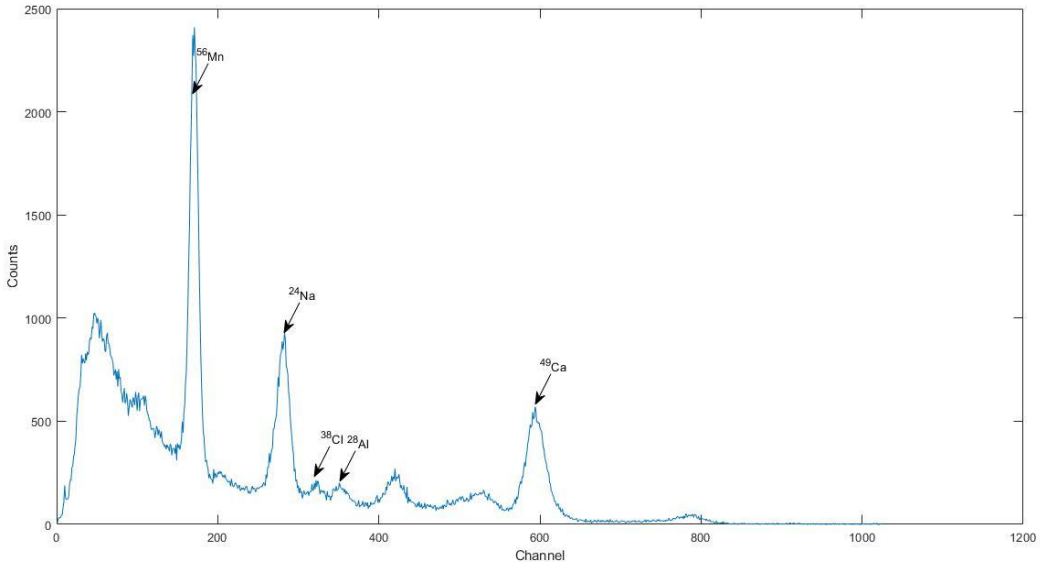

Figure 3.18 Spectrum acquired from participant P001 for the first 60s of counting

For P002, the spectrum appeared to have been spread out over a larger range of channels. However, the same peak patterns were still observed. In addition to the peaks being spread out, there were also large peaks ("noise", at ~0.205 MeV and ~0.770 MeV) present in the low energy region of the spectrum (see Fig 3.19) on the order of 10000 counts as opposed to 1000 counts in similar spectra. This may have been caused by detector gain fluctuations, though it is unclear. There was also a peak that was found at an energy of approximately 1073 keV, with a half life of 6.8 minutes. Looking at databases of radionuclides, it was initially thought this could be a Sr peak, though this suggestion was quickly eliminated as the Sr peak can only be made via a reaction with fast neutrons. The only other isotope with a similar half-life/energy combination is ^{66}Cu with a half-life of 5.1 minutes and an energy of 1039 keV, emitted in 9% of decays. While there are copper mines present in northern Ontario, given the amplitude of the peak, the amount of copper would have to be similar to that of the amount of calcium, something that may not be

physiologically possible. Unfortunately, there are no standards to compare to in order to figure out the actual concentration of the potential peak.

A potential other source of the Mn and Cu peaks could be from surface contamination. Cu is a common alloy used in gold jewellery in order to strengthen it, with even the purest of alloys only being 75% gold with the other 25% being Cu, Zn, Mn and other metals. While participants had any watches and/or jewellery removed prior to having their hands irradiated, residues from the metals may still have been present on the skin depending on the quality of the metal, though this seems unlikely. [16,17]

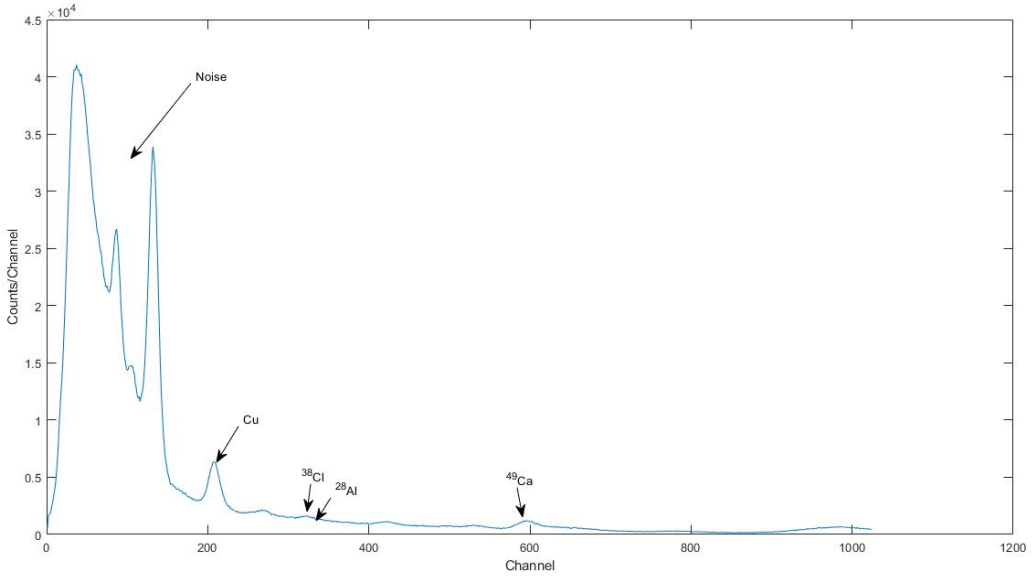

Figure 3.19 Spectrum acquired from Participant P002 for the first 60s of counting

While P003 did not show any abnormal peaks present, the collection system malfunctioned and initially only collected the first cycle of 60s. This was noticed approximately 5 to 6 minutes later

and the count was restarted. The first cycle was only analyzed as by the 5 to 6 minute mark almost 3 half-lives had passed.

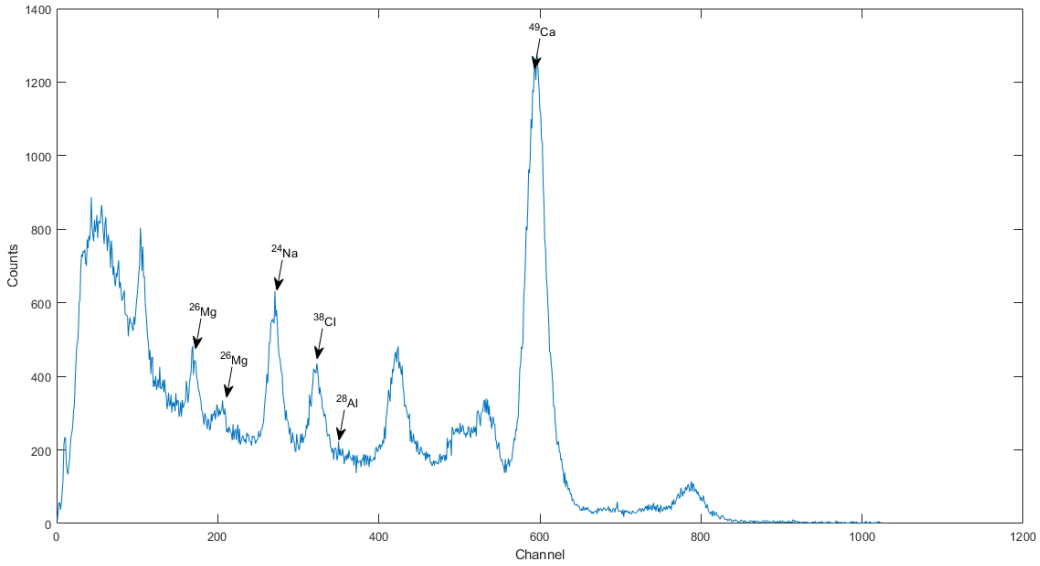

Figure 3.20 Spectrum acquired from Participant P003 for the first 60s of counting

3.3 Comparison with previous studies:

The mean concentration, highest values and inverse variance weighted mean values for the miner group, Alzheimer's Disease (AD) group and control group (AD and control values from [1]) can be found in the table below. A 2 sample independent measures t-test (Welch's test) was performed between the values for the Miner group and control group and miner group and AD group.

Table 3.6 Summary of Miner Values, compared with previous studies

	Highest Value (μgAl/gCa)	Mean Value (μgAl/gCa)	Inverse Variance Weighted Mean Value (μgAl/gCa)	Median (μgAl/gCa)
Miners (inverse variance weighted cycles)	206.36±14.76	17.43±13.78	21.78±2.27	18.56±11.28
Miners (summed cycles)	207.87±15.85	16.84±24.58	22.84±2.16	12.17±17.14
AD [1]	37.4±5.3	12.5±13.1	7.6±0.6	9.2
Control [1]	15.0±4.7	2.7±8.2	3.5±0.9	2.5

Table 3.7 Statistical Comparison of Miner Values with previous studies

	Highest Value (Miners vs Control)	Highest Value (Miners vs AD)	Mean Value (Miners vs Control)	Mean Value (Miners vs AD)	Inverse Variance Weighted Mean Value (Miners vs Control)	Inverse Variance Weighted Mean Value (Miners vs AD)
DF	16	17	22	27	18	15
t-value	47.8448	41.7257	3.5577	1.0042	28.9929	23.3916
alpha	0.05	0.05	0.05	0.05	0.05	0.05
p-value	<0.00001	<0.00001	0.0018	0.3242	<0.00001	<0.00001

The highest valued participant in [1] was 37.4±5.3μgAl/gCa, approximately five times less than the reported 206.36±14.76 μgAl/gCa for subject P001 from this study. These values are significantly different with a p-value of <0.00001, suggesting either that the inhaled Al stays in the body much longer than environmental exposure or that the initial exposure was significantly greater. It should also be noted that while exposure levels for each miner varied, this was a blinded study, for which the key has not been provided to determine whether bone level corresponds to length of work or estimated exposure level. The differences between the Miners

and the control group is even larger than the AD group, being almost 13 times larger than the control group, being significantly different with a p-value <0.00001. Reasons for the large differences in concentration at this point seem most likely due to the McIntyre Powder the miners were required to inhale. However, as it is not possible at this point to determine whether Al bone level is correlated with exposure, this is not confirmed.

3.4 Issues

For the first sample of 5000 μg Al, the first 60s cycle seemed to be the sum of the first ten cycles. In order to account for this a correction factor was implemented. The correction factor was calculated by using the radioactive decay formula $N = N_o e^{-\lambda t}$ and applied to the data before fitting. This issue seems to have been an error in the data collection electronics for the 4π rather than the phantom itself as the same phantom, irradiated under the same conditions, did not produce such large peaks for the first 60s for either the $LaBr_3$(Ce) and HPGe detectors.

Another issue present was with P001. There was an issue with the seal of the water bag, resulting in a dose of 2.5 mR to the participant due to neutron leakage around the arm.

Other issues include having issues with fitting the calcium peaks, as the observed long tails seemed to greatly increase the chi-square of the fits.

3.5 Conclusions:

While these results are not possible to fully interpret at this time, in absence of the exposure 'key', it does not come as much of a surprise that some miners have observable Al in bone, while many are below the detection limit. Many of these miners have not been exposed to high levels of aluminum in more than 40 years (the last recorded use of McIntyre powder was in the 1970s), and aluminum is said to have a biological half-life of 10 to 20 years [40] meaning anywhere

from 2 to 4 biological half-lives have passed. Even with exposure as a factor, it might be expected that a number of them did not have detectable levels of aluminum.

For initial exposure, assuming the last miner was exposed at the end of the McIntyre powder era (~1980), and the half-life is 10 to 20 years, then a total of 2 to 4 half lives have passed, meaning that a correction factor of 2^2 or 2^4 needs to be applied. If we look at the highest value (206.36 μgAl/gCa) then the highest value in 1980 would have been 3301.76 μgAl/gCa, and the lowest would be 825.44 μgAl/gCa.

In the late 1980s, Ellis *et al* [38,39] reported Al levels in dialysis patients who had been exposed to Al, but not shown any symptoms related to any Al diseases. They utilized the epithermal/thermal neutron beam from the Brookhaven National Laboratories reactor in order to find the concentration of Al in the hand of the patients. The highest reported level was stated at 0.76 mgAl/gCa, or 760 μgAl/gCa. It is assumed that these patients were irradiated in a time period where biological elimination of Al would have been negligible, therefore we can assume that the levels are similar to that of their initial exposure.

When compared with the range of the highest initial exposure (825.44μgAl/gCa – 3301.76μgAl/gCa) of the miner group, the values are either similar (in the case of 825.44μgAl/gCa) in value, or 4 times larger (in the case of 3301.76 μgAl/gCa). This suggests that the highest values of Al measured in this set of miners is abnormally high, and further suggests that bone Al measurements are a good way of measuring exposure of inhaled Al.

Chapter 4: Investigation Into Alternate Detectors to Measure *in-vivo* Al Levels

As stated in Chapter 1, a major disadvantage of the NaI(Tl) scintillator is its poor resolution, which results in the overlap of the 1.64 MeV ^{38}Cl peak with the 1.78 MeV ^{28}Al peak. For other detector options we want to have something that can achieve a similar (or better!) MDL, similar efficiency and better resolution.

4.1 Lanthanum Bromide

4.1.1 Lanthanum Bromide Natural Radioactivity

Since lanthanum is naturally radioactive, there is a prominent peak at 1436 keV from naturally occurring radioactive ^{138}La (0.09% of all naturally occurring lanthanum).

Figure 4.1: Spectrum for a 2000 μg Al phantom for the $LaBr_3$(Ce) detector

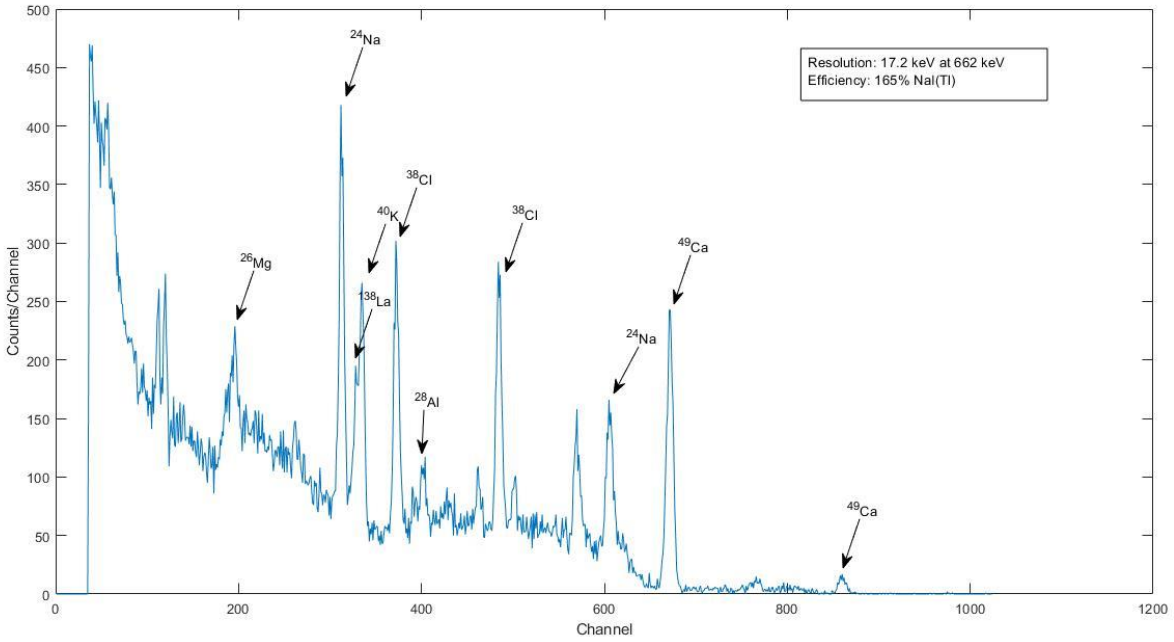

For our measurements the 1436 keV peak does not overlap with either the 1.78 MeV ^{28}Al peak or the 3.08 MeV ^{49}Ca peak, therefore this does not interfere directly with our analysis, and can thus be ignored. However, if one wanted to model a complete detector response then this peak would need to be included, which has the potential to negatively impact the fit if it is not fit properly.

4.1.2 Resolution:

The resolution of the $LaBr_3$(Ce) detector was found to be 1.98% at 1.332 MeV or 26.5 keV at 1.332 MeV.

A big advantage of the $LaBr_3$(Ce) crystal is the resolution. While the resolution of the NaI(Tl) was 4.69% at 1.64 MeV, even with anti-coincidence rejection there was still significant overlap between the ^{28}Al and ^{38}Cl peaks. With the lanthanum, however, the two peaks were distinct, though there was still a small overlap in the tails, meaning that one fit with two gaussians is still advised. While the fitting algorithm did not work for these experiments, the peaks were distinct enough that manual fitting was able to be performed, something that would have been too cumbersome for the NaI(Tl) system. Another advantage of the lanthanum is its more compact size compared to the NaI(Tl), allowing for the setup to occupy less space.

4.1.3 MDL:

Table 4.1: Areas of the first 60s cycle of counting Al phantoms with varying concentrations for the $LaBr_3$(Ce) detector

Phantom	Al Area	Ca Area	Al/Ca
0_1	72.00±16.97	894.55±45.97	0.0805±0.0194
0_2	23.75±13.28	542.20±35.81	0.0438±0.0247
250_1	-13.40±19.26	763.45±40.94	-0.0175±0.0252
250_2	26.50±19.98	786.65±41.94	0.0337±0.0255
500_1	30.00±43.22	684.80±38.91	0.0438±0.0632
500_2	26.33±24.66	685.10±38.47	0.0384±0.0360
750_1	105.90±44.07	712.60±40.30	0.1486±0.0624
750_2	31.60±33.63	415.30±30.06	0.0761±0.0812
1000_1	7.00±44.89	779.00±43.45	0.0090±0.0576
1000_2	312.90±38.83	824.40±42.52	0.3795±0.0510
2000_1	118.20±44.46	591.75±36.30	0.1997±0.0761
2000_2	86.00±47.42	736.75±40.50	0.1167±0.0647
5000_1	202.00±59.42	712.35±39.23	0.2836±0.0848
5000_2	197.00±50.25	489.9±33.38	0.4021±0.1062
10000_1	382.60±50.22	658.15±40.10	0.5813±0.0841
10000_2	531.20±55.00	859.55±46.10	0.6180±0.0721
25000_1	1394.80±68.56	854.80±46.61	1.6317±0.1184
25000_2	896.90±57.90	642.60±38.16	1.3957±0.1224
50000_1	1842.40±71.57	652.15±38.01	2.8251±0.1979
50000_2	2178.50±79.97	799.20±43.61	2.7259±0.1764

Table 4.2: Areas of the second 60s cycle of counting Al phantoms with varying concentrations for the $LaBr_3$(Ce) detector

Phantom	Al Area	Ca Area	Al/Ca
0_1	26.75±16.24	736.10±42.32	0.0363±0.0222
0_2	18.25±13.26	532.05±34.98	0.0343±0.0250
250_1	-51.70±18.51	747.30±41.04	-0.0692±0.0248
250_2	24.50±19.84	724.25±40.64	0.0338±0.0275
500_1	35.40±39.83	623.35±37.72	0.0568±0.0632
500_2	55.33±27.52	593.40±36.43	0.0932±0.0467
750_1	6.80±42.88	642.10±37.92	0.0106±0.0668
750_2	28.50±25.91	343.75±28.66	0.0829±0.0757
1000_1	-153.30±52.62	717.75±40.75	-0.2136±0.0743
1000_2	158.5±51.22	772.50±41.03	0.2052±0.0672
2000_1	61.50±41.89	586.25±36.48	0.1049±0.0718
2000_2	127.00±47.24	727.25±39.75	0.1746±0.0657
5000_1	175.00±56.50	662.25±37.90	0.2643±0.0866
5000_2	187.10±48.76	478.10±32.83	0.3913±0.1055
10000_1	304.70±48.55	696.95±40.36	0.4372±0.0741
10000_2	386.70±51.06	754.70±43.85	0.5124±0.0739
25000_1	832.50±62.82	732.80±44.48	1.1361±0.1100
25000_2	673.20±52.03	556.35±36.32	1.2100±0.1224
50000_1	1335.00±63.28	654.65±38.66	2.0393±0.1544
50000_2	1587.80±71.33	757.80±41.84	2.0953±0.1391

Table 4.3: Areas of the third 60s cycle of counting Al phantoms with varying concentrations for the $LaBr_3$(Ce) detector

Phantom	Al Area	Ca Area	Al/Ca
0_1	36.00±17.66	686.40±40.73	0.0524±0.0259
0_2	13.50±12.98	456.95±32.93	0.0295±0.0285
250_1	-14.00±18.51	646.90±38.75	-0.0216±0.0286
250_2	32.00±20.42	639.05±38.02	0.0501±0.0321
500_1	50.40±40.20	618.50±37.05	0.0815±0.0652
500_2	7.10±39.44	570.80±35.87	0.0124±0.0691
750_1	-17.60±42.71	611.75±37.17	-0.0288±0.0698
750_2	14.50±23.43	344.05±27.33	0.0421±0.0682
1000_1	8.20±39.38	652.15±38.56	0.0126±0.0604
1000_2	40.70±47.61	725.05±40.22	0.0561±0.0657
2000_1	51.60±42.01	527.50±34.31	0.0978±0.0799
2000_2	122.80±45.45	605.50±36.95	0.2028±0.0761
5000_1	112.70±55.00	651.00±37.82	0.1731±0.0851
5000_2	158.00±48.01	469.75±31.93	0.3363±0.1047
10000_1	195.10±44.92	643.20±38.55	0.3033±0.0722
10000_2	223.90±48.48	736.95±43.03	0.3038±0.0681
25000_1	664.30±58.04	739.35±42.75	0.8985±0.0941
25000_2	398.30±48.17	466.10±34.27	0.8545±0.1209
50000_1	952.80±57.43	578.20±35.82	1.6479±0.1424
50000_2	1232.80±63.88	664.70±38.75	1.8547±0.1447

The MDL for the lanthanum bromide was calculated using the procedure in Section 2.13 by taking the average of the uncertainties for the low concentration phantoms as 98.67μgAl/gCa, or 1470.20 μg Al.

4.1.4 Issues:

The naturally occurring ^{138}La peak has the potential to obscure or overlap with other elements in the spectrum, which could potentially lead to a decrease in the fitting precision. While the presence of the x-rays caused issues initially (due to their amplitude obscuring the rest of the spectrum, see Fig 2.1), they are a low enough energy that should they be present in future acquisitions, they can simply be cut out of the spectrum before analysis begins.

4.2 HPGe

Due to the fitting algorithm having trouble with the low background of the germanium spectra, manual fitting was performed. This was most likely due to the zero values causing the chi-square to have a divide by zero error. Also, since each cycle had such low counts/channel, the first three cycles were summed before analysis.

4.2.1 Resolution:

The main advantage of the germanium detector is its excellent resolution, at 0.136% (1.81 keV) at 1.332 MeV. The ^{28}Al and ^{38}Cl peaks are fully resolved (with at least a few hundred channels between them, as well as between the aluminum peak and any other adjacent peaks that could not be resolved by either the lanthanum or sodium iodide detectors. One can also get more information out of a germanium detector spectrum, as compared to the $LaBr_3$(Ce) and NaI(Tl), such as escape peaks (see Figure 4.2). This can, in theory, allow for a greater accuracy in calculating the concentration of Al (or any other element) as one can now take into account some escaped photons that did not deposit themselves into the main photopeak.

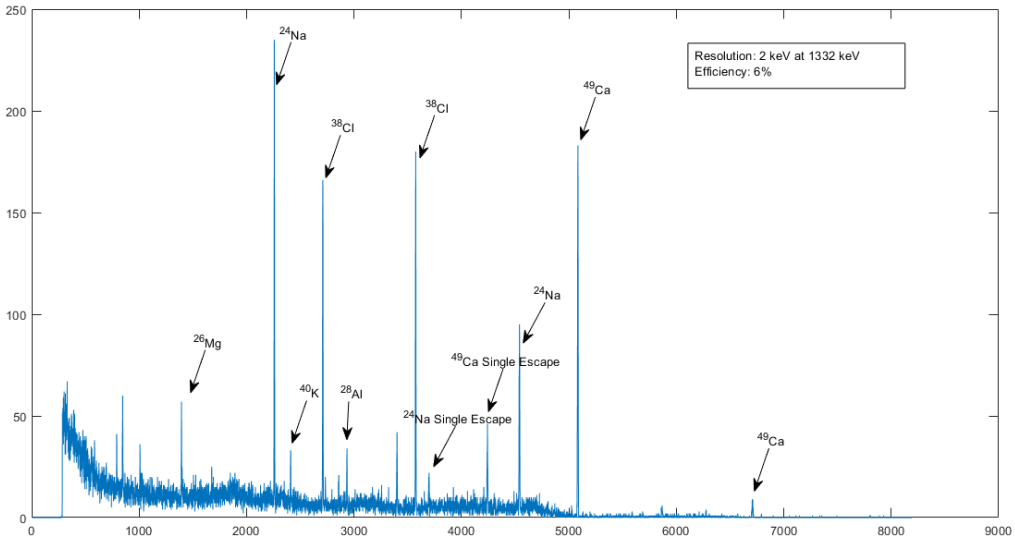

Figure 4.2: Spectrum for a 5000µg Al phantom taken on an HPGe detector. x-axis is channel, y-axis is counts.

Since the resolution of the HPGe is so high, this causes the peaks to become quite narrow One issue that arises with the Germanium is since it does have such a high resolution, this makes the peaks quite narrow, even when using the optimal gain settings, meaning that a large amount of data is compressed into a small amount of channels, which can lead to issues with fitting.

The main disadvantage of the Germanium detector as compared to the other two is its efficiency. Solid state detectors in general have much lower efficiencies than scintillators, which leads to less of the photons emitted by the source being counted and therefore less information.

Table 4.4: Areas for phantoms of varying Al concentrations for the sum of the first 3 60s cycles for the HPGe detector

Phantom	Al Area	Ca Area	Al/Ca
50000_1	2756.00±58.55	1300.50±41.79	2.1192±0.0816
50000_2	2663.00±58.55	1236.50± 38.45	2.1536±0.0820
25000_1	1288.50± 41.87	976.00±37.74	1.3202±0.0667
25000_2	1468.00±49.34	1272.00±42.99	1.1541±0.0550
10000_1	632.50±36.22	1322.00±38.52	0.4784±0.0307
10000_2	555.50±31.94	1401.00±41.10	0.3965±0.0256
5000_1	281.00±32.57	1295.00±38.17	0.2170±0.0259
5000_2	223.00±22.20	995.00±36.81	0.2241±0.0238
2000_1	117.00±23.17	1300.00±38.00	0.0900±0.0181
2000_2	123.00±21.92	1145.50± 38.27	0.1074±0.0195
1000_1	143.00±20.87	1206.00±45.50	0.1186±0.0179
1000_2	71.00±25.61	1214.00±38.76	0.0585±0.0212
750_2	116.00±21.26	1276.00±41.33	0.0909±0.0169
500_1	85.00±19.62	1338.00±39.42	0.0625±0.0148
500_2	116.00±22.33	1093.00±35.42	0.1061±0.0207
250_1	30.00±21.42	1038.00±34.63	0.0289±0.0207
250_2	41.00±12.69	939.00±31.80	0.0437±0.0136
0_1	11.50±20.12	1015.50± 39.98	0.0113±0.0198
0_2	6.00±17.49	998.00±35.86	0.0060±0.0175

The MDL for the single germanium detector was calculated as 56.51 μgAl/gCa, or 842.02 μg Al. This is approximately half the MDL of the $LaBr_3$(Ce), but still 2.5 times larger than the in-vivo MDL for the NaI(Tl) and 3 times the phantom MDL for the NaI(Tl).

4.3 Solid Angle Calculation and MDL improvement

Following the procedure from Section 2.14, the solid angle for the germanium and lanthanum detectors were calculated by first calculating the solid angle of a point source, then extrapolating from there. All sources were assumed to be the same average distance from the detector face, with the distance between the edge of the bottle and the detector face approximately 0.5cm (some bottles were further from the detector face than others).

For the germanium detector the average solid angle over the volume was found to be 0.2959 [sr/cm^3], and for the lanthanum was found to be 0.2959 [sr/cm^3].

Since a 4π system for either is only semi-plausible a two detector system is only being considered. For the lanthanum this two detector system leads to the solid angle being 0.5918, with an improvement of $\frac{1}{\sqrt{2}}$ in the MDL. This leads to an MDL of 69.77 μgAl/gCa or 1039.58 μgAl, a factor of 6.23 times greater than the MDL of the 4π system. For the HPGe system, the MDL with 2 detectors would equal 39.96 μgAl/gCa, a factor of 2.50 greater than the 4π. The improvement factor comes from the ratio of solid angle improvement, for each detector you get an improvement of $\frac{1}{\sqrt{n}}$ where n is number of detectors.

As can be seen from the above two cases, adding even one more detector greatly improves the MDL's of both systems, though it may not be as precise as the NaI(Tl) this shows that you can still get a reasonable MDL, though not for the lanthanum, as the lowest amount found was 18.5±3.9 μgAl/gCa. In order to achieve this for either system one would need to have 9 HPGe detectors (or 3 to 4 HPGe detectors with double the volume), or 16 $LaBr_3$(Ce) detectors. One thing to note is that this does not take into account anti-coincidence and coincidence counting techniques, which are used for the NaI system to supress the coincidence summing effects of the Cl peaks. If this is implemented with multiple HPGe or $LaBr_3$(Ce) detectors it may further improve the detection limit.

MDLs for both the $LaBr_3$(Ce) and HPGe were calculated by taking the average of the uncertainties for the low concentration phantoms (0 to 2000 μg). These values were then divided by the slope for each cycle (i.e. if the average uncertainties for cycle 1 were taken this value was

divided by the slope for cycle 1). These values were then added via inverse variance weighted mean method. This value was then multiplied by 2 to finally get the MDL for the system.

	NaI	HPGe	$LaBr_3(Ce)$
MDL (μg Al)	236.17- phantoms	842.02	1470.20
MDL (μg Al/g Ca)	22.57 – in-vivo 15.85 - phantoms	NA 56.51 - phantoms	NA 98.67 - phantoms

Table 4.5: Summary of MDL values for all three detector types, given in ug Al and μg Al/gCa.

As can be seen from the above table (4.5), the MDLs for the $LaBr_3(Ce)$ and HPGe detectors are significantly larger than those of the 4π NaI detector. However, as noted above, a multi-detector array would decrease the MDL, by a factor of 1/sqrt(n), and for some setups is feasible. From these data the most feasible economically would be the HPGe as it would require less detectors to achieve the same phantom MDL (12 small volume, or 3 to 4 large volume) or 36 for the $LaBr_3(Ce)$.

	NaI(Tl) 4π	HPGe	$LaBr_3(Ce)$
Density	Different for each detector	5.323 g/cm^3	5.08 g/cm^3
Peak Resolution (stated)	Different for each detector	2keV at 1332 keV 0.15% at 1332 keV	2.6% at 662 keV 17.2 at 662 keV
Intrinsic Efficiency (Total)	0.5 (50%) over 1.5 MeV	30% of NaI(Tl) [30] ~6%	165% singular NaI(Tl) [37]
Peak Resolution (measured)	4.69% at 1.64 MeV 77.0 keV	0.136% at 1332 keV 1.8keV	1.98% at 1332 keV 26.5 keV at 1332 keV
Solid Angle	~4π [sr]	0.2959 [sr cm^{-3}]	0.2959 [sr cm^{-3}]

Table 4.6: Comparison of properties of all three detector types.

As can be seen from the above tables and graphs, both the $LaBr_3(Ce)$ and HPGe detectors show significant improvements in the resolution of the Al spectrum compared to the NaI(Tl). Both are able to resolve the Al and Cl peaks, though the HPGe is able to resolve it fully, while the $LaBr_3(Ce)$ has the tails overlap. The efficiency of the singular $LaBr_3(Ce)$ is better than that of the HPGe, but not of the 4π. However, if multiple $LaBr_3(Ce)$ detectors were present then this could

improve the efficiency to be greater than that of the 4π. For the HPGe even with multiple detectors the efficiency will most-likely never end up as good as that of a scintillator, though it can still be greatly improved.

As for choosing a detector set-up, either detector could work as both are able to resolve the Cl and Al peaks, though the HPGe has the advantage as it fully resolves the two peaks. The biggest limiting factor would most likely be price as the $LaBr_3$(Ce) is much more expensive than the HPGe. Other options that could work include using less, but higher volume detectors.

When choosing a set of detectors it comes down to efficiency vs resolution, if one were to want the peaks fully resolved then the HPGe would be the better candidate as the significant amount of channels between peaks means one is guaranteed to have no interference between the Al and Cl peaks. However if one were to want a greater efficiency, then the $LaBr_3$(Ce) setup would be a better choice.

4.4 Comparison with Previous Studies

At Purdue university two different studies were conducted using an HPGe detector, the first one [34] utilized tissue-equivalent phantoms to design a compact deuterium-deuterium (DD) IVNAA system for use with human subjects. In it, an MDL of 11.13 μgAl/gdry bone (44.5 μgAl/gCa) was achieved. In comparison with phantom data from this thesis, 56.41 μgAl/gCa, the value achieved here was above that of Byrne et al with a percent difference of 26.8%. However it should be noted the HPGe detector they were using was 100% efficient, where as ours is 30% efficient (of a NaI(Tl) crystal).

The second study was conducted by Hasan et al [33], again using a compact DD IVNAA system, on a sample of 43 Chinese miners who were exposed to Al when working in manufacturing and

ferroalloy facilities. For this group an in-vivo MDL of ~63 μgAl/gCa dry bone, or 248.09 μgAl/gCa was achieved, and a dose to the hand was 11.9 mSv compared with ~210 μSv with our study. When compared to the 56.51 μgAl/gCa MDL of the single HPGe detector, the MDL of the HPGe is significantly less (approximately 4 times) than the in-vivo MDL, meaning that there is a potential for this single HPGe detector to reliably measure in-vivo Al.

We can apply a correction factor of $\frac{1}{\sqrt{3.33}}$ to compensate for the differences in efficiencies and get that the adjusted MDL would be 30.91 μgAl/gCa, less than the 44.5 μgAl/gCa from Byrne et al suggesting again that this setup can reliably measure Al in-vivo, and if an identical setup to Byrne et al was used then the results achieved would be similar.

4.5 Conclusion

Both the HPGe and $LaBr_3$(Ce) showed improved resolution over the NaI(Tl), with both being able to resolve the Al and Cl peaks, though the $LaBr_3$(Ce) did have the tails of the two peaks overlap while the HPGe did not. However, despite both the HPGe having lower efficiency compared to the $LaBr_3$(Ce), the MDL for it was significantly less, and therefore better, than the $LaBr_3$(Ce), suggesting that the HPGe would be the better option for detecting Al in-vivo.

The HPGe also has another significant advantage over the $LaBr_3$(Ce) and NaI(Tl) as there is little to no gain drift and with multiple detectors independent gains for each detector would be feasible.

Compared with previous studies with a significantly lower neutron dose to the hand, and despite having a detector with ~3.33 times less the efficiency, the values obtained for MDL for the HPGe were still close to the in-vivo and in-vitro values.

4.6 Future Work:

Future work for this part of the project would be using multiple HPGe and $LaBr_3$(Ce) detectors to see how large the MDL improvement was. When a suitable system is found, then in-vivo measurements may be able to be performed and compared to in-vivo measurements from the NaI(Tl) studies. This could lead to a much higher accuracy in the measurement of the concentration of Al in the human body, which could in turn lead to a better understanding of Al in the bone.

Chapter 5: Conclusions and Future Work

5.1 Conclusions

The maximum detected concentration of Al in bone in a volunteer from the miner population was 206.36+/-14.76 μgAl/gCa. This level is significantly greater than zero and is high compared to previously published data. In addition, a further 6 of the 15 miners had detectable Al levels i.e. they had concentrations of Al in bone greater than the MDL of the 4π system. As expected, there were slight differences between in vivo and phantom MDLs. The value for the phantom MDL was calculated as 15.85 μgAl/gCa (236.17 μgAl), while the MDL drawn from in-vivo data was calculated to be 22.57 μgAl/gCa. Living humans have more variability in bone density than phantoms, more tissue overlay and they can move, which are all factors which tend to worsen precision.

When compared with previous data, these values were found to be significantly higher, with a broader range of values,suggesting that initial exposure levels were much higher for the miner group compared to the AD group. At this time, however, cognitive testing results have not been made available so it is not possible to determine whether level of Al exposure can be associated with cognitive impairment. Furthermore, the exposure 'key' has not yet been made available and it is not possible to determine whether bone Al levels are associated with working history or other predictors of exposure.

The MDLs of the HPGe and $LaBr_3$(Ce) detectors were determined to be 56.51 μgAl/gCa (842.02 μgAl) and 98.67 μgAl/gCa (1470.20 μgAl) respectively. A significant factor in the poorer precision of these detectors compared to the 4π NaI(Tl) detector array is the lower geometric efficiency. These detectors subtend a far smaller angle than the 4π.

The solid angles of the $LaBr_3$(Ce) and HPGe were found to be the same and were calculated as 0.2959 [sr/cm^3] as compared to the 3.87π [12,13] for the 4π

Both the $LaBr_3$(Ce) and HPGe detectors showed an improved resolution, but lower efficiency when compared to the 4π. However, the efficiency could be easily fixed by creating arrays of more detectors. For the LaBr3 in order to achieve results similar to the 4π system, a factor of 36 times the number of detectors would be needed.

For the HPGe, an array of 12 of the single volume detectors are needed, or an alternative would be an array of 3 to 4 large volume detectors, at an estimated cost of $250000 to $1.1M.

The HPGe detector seems to show the most promise, as MDLs for this are similar in scope to that which was achieved by [38,39] in 1987. The MDL for the phantoms studied here was also lower than the MDL for the published in-vivo MDL for [38,39].

However, the process performed here was not without errors. One of the largest sources of error that could contribute to the uncertainties in the data would be that for each calibration of the 4π system, there would be one detector (in most cases detector 9, which was located at the back of the cavity) whose gain would fluctuate significantly throughout the course of the experiment. This could in turn affect the location of the peak energy, and therefore the number of counts under the curve.

With the measurements of the miners there were a few issues as well. First being that, due to the short half-life of ^{28}Al, the miners who had the longer transfer time may have lost counts under the peak due to longer decay. This was corrected for, the fix for this being a simple one, however, and one can simply multiply by a correction factor equal to difference in time between

the start of the calibration curve counting time from the miner counting time. However, this does mean that miners with longer transfer times likely had poorer precisions.

Another issue present was specifically with the measurements of subjects P003 and P004. With subject P003, the counting system stopped counting after the first cycle. This was thought to be due to having selected the 'Display graph after every cycle' execution choice. For subject P004, the wrong arm was placed in the detector for the first 3 to 4 cycles, to mitigate the effects of this mistake, cycles 4 to 6 were taken as the first three cycles.

5.2 Future Work:

In the future, multiple HPGe, or large volume HPGe detectors may be investigated to see if the MDL can be improved further as indicated by this work. If a significant improvement is found, then in-vivo experiments, or *ex-vivo* experiments on bone samples, could be investigated to see if the in-vivo MDL for Al could be improved even further. Including spectral decomposition as the method of analysis for the HPGe and $LaBr_3$(Ce) detectors could be useful in addition to seeing the results for multiple lanthanum bromide and germanium detectors. For fitting the data a Lorentzian instead of a Gaussian model for the peaks could also be looked at to see if that could further improve the fit for the 4π detector.

Appendix:

Table A1: Quantities of salts for first set of Al phantoms

$AlNO_3$ (mL)	$MgNO_3$ (g)	$CaCO_3$ (g)	$ClNH_4$ (g)	$NaNO_3$ (g)
0	2.3209	87.68	1.78	4.62
0.250	2.37	87.73	1.81	4.65
0.500	2.35	87.73	1.84	4.64
0.750	2.31	87.73	1.79	4.64
1.000	2.29	87.80	1.80	4.73
2.000	2.36	87.76	1.81	4.63
5.000	2.27	87.84	1.80	4.62
10.000	2.33	87.60	1.77	4.64
25.000	2.35	87.77	1.84	4.59
50.000	2.31	87.82	1.79	4.63

Table A2: Quantities of salts for second set of Al phantoms

$AlNO_3$ (mL)	$MgNO_3$ (g)	$CaCO_3$ (g)	$ClNH_4$ (g)	$NaNO_3$ (g)
0	2.31	87.74	1.83	4.61
0.250	2.31	87.84	1.80	4.62
0.500	2.39	87.83	1.78	4.62
0.750	2.30	87.79	1.80	4.76
1.000	2.29	87.86	1.87	4.64
2.000	2.30	87.81	1.81	4.64
5.000	2.34	87.76	1.78	4.66
10.000	2.34	87.86	1.78	4.74
25.000	2.37	87.77	1.83	4.63
50.000	2.33	87.88	1.80	4.61

References:

[1] Mohseni, Hedieh, K. et al, "A Pilot Study Measuring Aluminum in Bone in Alzheimer's Disease and control Subjects Using *in vivo* Neutron Activation Analysis" *Journal of Alzheimer's Disease* vol. 53, 2016, pp. 933-942.

[2] Comsa, D.,C., et al "Application of spectral decomposition analysis to in vivo quantification of aluminum by neutron activation analysis", *Applied Radiation and Isotopes* vol 61, 2004, pp. 1353-1360.

[3] Lavergne, Valery, et al. "Risk factors and consequences of hyperaluminemia in a peritoneal dialysis cohort", *Peritoneal dialysis international :Journal of the International Society for Peritoneal Dialysis* vol. 32, no. 6, 2012, pp. 645-51.

[4] Pacific Northwest National Laboratory, Department of Energy. "Comparison of LaBr3:Ce and NaI(Tl) Scintillators for Radio-Isotope Identification Devices (Revision 0)", April 2006. https://www.pnnl.gov/main/publications/external/technical_reports/PNNL-15831.pdf. Accessed 2018.

[5] Underwood, E.,J., Trace Elements in Human and Animal Nutrition. 5, Waltermertz, 1956. Print.

[6] Pieredes, A.,M., et al "Hemodialysis encephalopathy with osteomalacic fractures and muscle weakness" *Kidney International,* vol 18, no. 1, 1980, pp. 115-124.

[7] Department Of Health And Human Services, Public Health Service Agency for Toxic Substances and Disease Registry. "Public Health Statement: Aluminum, CA # 7429-90-S", September, 2008. https://www.atsdr.cdc.gov/ToxProfiles/tp22-c1-b.pdf. Accessed 2019.

[8] Arnold, L. J., et al. "Portable gamma spectrometry with cerium-doped lanthanum bromide scintillators: Suitability assessments for luminescence and electron spin resonance dating applications", *Radiation Measurements,* vol. 47, no. 1., 2012, pp. 6-18.

[9] Rifat, S. L., et al. "Effect of exposure of miners to aluminium powder", *The Lancet,* vol. 336, no. 8724, 1990, pp. 1162-1165.

[10] Radiation Detection and Measurement, Knoll, Glenn, F. John Wiley & Sons. 2000

[11] Atoms, Radiation, and Radiation Protection, by James E. Turner, Wiley-VCH.

[12] Byun, S. H., et al. "4 π NaI(Tl) Detector Array for In Vivo Neutron Activation Analysis", *IEEE Transactions On Nuclear Science,* vol. 53, no. 5, 2006, pp. 2944-2947.

[13] Byun, Soo Hyun. Radioisotopes and Radiation Methodology. McMaster University. Engineering Rechnology Building. September 2017 – March 2018. Lecture.

[14] Obložinsky, P and I. Ribanský. "The solid angle subtended at a disk Source by a non-parallel disk detector", *Nuclear Instruments and Methods,* vol. 94, no. 1, 1971, pp. 187-188.

[15] "Office of Dietary Supplements - Manganese." *NIH Office of Dietary Supplements*, U.S. Department of Health and Human Services, ods.od.nih.gov/factsheets/Manganese-HealthProfessional/#en2.

[16] "Buying Sterling Silver Jewellery - Working Silver: Jewelry Making Tools & Supplies." *Working Silver | Jewelry Making Tools & Supplies*, 16 June 2016, workingsilver.com/buying-sterling-silver-jewellery/. Accessed Mar 2020

[17] Whiteflash. "Whiteflash." *An Overview Of Common Alloys Used In Jewelry*, 18 May 2016, www.whiteflash.com/about-diamonds/jewelry/an-overview-of-common-alloys.htm. Accessed Mar 2020

[18] Ott, S. M., et al. "Aluminum is associated with low bone formation in patients receiving chronic parenteral nutrition", *Annals of Internal Medicine*, vol. 98, no. 6, 1983, pp. 910–914.

[19] Zarnke, Andrew, et al. "Physical and chemical characterization of McIntyre Powder: An aluminum dust inhaled by miners to combat silicosis", *Journal of Occupational and Environmental Hygiene*, vol. 16, no. 11, 2019, pp. 745-75.

[20] Burwen, Dale R. et al. "Epidemic aluminum intoxication in hemodialysis patients traced to use of an aluminum pump", *Kidney International*, Vol. 48, no. 2, 1995, pp. 469-474.

[21] Alfrey, A. C. et al. "The dialysis encephalopathy syndrome. Possible aluminum intoxication". *New England Journal of Medicine*, vol.. 294, 1976, p. 184.

[22] Williams, Y.,R., "Whole body aluminum in chronic renal failure and dialysis encephalopathy" *Clinical Nephrology*, vol 18, no. 4, 1980, pp. 198-200.

[23] Martin, C. W., and the WorkSafeBC Evidence-Based Practice Group. *Occupational Exposure to Aluminum (McIntyre Powder) by Inhalation and the Development of Neurological Disorders.* Richmond BC: WorksafeBC, Evidence-Based Practice Group, 2017.

[24] Verma, Dave K. "Aluminum in the lungs of Ontario hardrock miners", *Archives of Environmental & Occupational Health*, vol. 75, no. 2, 2020, pp. 75-78.

[25] McDonald, B., et al. "A mortality study of Alzheimer's disease and aluminium exposure through inhalation of McIntyre powder in Cornish Tin Miners", *Neurobiology of Aging*, vol. 17, no. 4 Supplement 1, 1996, pp. S122-S123

[26] Wyatt, R., M. et al, "The development of a technique to measure bone aluminum content using neutron activation analysis" *Physiological* Measurement, vol 14, no 3, 1993, pp. 327-335

[27] S.Y.F. Chu, L.P. Ekström and R.B. Firestone, *WWW Table of Radioactive Isotopes*, database version 1999-02-28 from URL http://nucleardata.nuclear.lu.se/nucleardata/toi/ - for general

[28] Davis, K et al. "*In vivo* measurement of bone aluminum in population living in southern Ontario, Canada" *Medical Physics*, vol 35, no. 11, 2008 pp 5115-5123.

[29] "Welding and Manganese" *The National Institute for Occupational Safety and Health* U.S. Department of Health & Human Services https://www.cdc.gov/niosh/topics/welding/default.html 2013Accessed Mar 2020.

[30] Canberra Industries Inc. (2003). "Germanium Detector: User's Manual", Print. Meriden CT.

[31] "Periodic Table of Elements and X-ray Energies". *Bruker* https://www.bruker.com/fileadmin/user_upload/8-PDF-Docs/X-rayDiffraction_ElementalAnalysis/HH-XRF/Misc/Periodic_Table_and_X-ray_Energies.pdf. 2020

[32] Chettle, David et al. "A pilot study measuring aluminum stored in bone and assessing cognitive function in former mine workers who were exposed to McIntyre powder". Ethics guideline document. August 26 2019. Electronic Document.

[33] Hasan, Zainab, et al "Characterization of bone aluminum, a potential biomarker of cumulative exposure, within an occupational population from Zunyi, China" *Journal of Trace Elements in Medicine and Biology* vol. 59, 2020, pp. 1264-69.

[34] Byrne, Patrick et al. "The study of *in vivo* quantification of aluminum (Al) in human bone with a compact DD generator-based neutron activation analysis (NAA) system" *Physiological Measurement,* vol 37, 2016, pp. 649-660.

[35] *Gamma-Ray Coincidence Counting Techniques.* Mirion Technologies. https://www.mirion.com/learning-center/lab-experiments/gamma-ray-coincidence-counting-techniques-lab-experiment

[36] Crystals Saint-Gobain. *Coincide/Anti-coincidence: Detector Applications Information Note* Saint-Gobain Ceramics & Plastics, Inc, 2004-2016. https://www.crystals.saint-gobain.com/sites/imdf.crystals.com/files/documents/coincidence-anti-coincidence-application_70279.pdf. Accessed 6 Apr 2020.

[37] Crystals Saint-Gobain. *Lanthanum Bromide and Enhanced Lanthanum Bromide data sheet.* Saint-Gobain Ceramics & Plastics, Inc, 2004-2017. https://www.crystals.saint-gobain.com/sites/imdf.crystals.com/files/documents/lanthanum-material-data-sheet.pdf. Accessed Mar 2020.

[38] Ellis, K J, and Kelleher, S P. *In vivo bone aluminum measurements in patients with renal disease*. United States: N. p., 1986. Web.

[39] Ellis, K. J., et al, "In vivo monitoring of skeletal aluminum burden in patients with renal failure"*Journal of Radioanalytical and Nuclear Chemistry* vol. 124, no. 1, 1988 pp. 85-95

[40] Priest, N.D., "The biological behaviour and bioavailability of aluminum in man, with special reference to studies employing aluminum-26 as a tracer: review and study update" *Journal of Environmental* Monitoring. Vol 6, no 5, 2004, pp. 275-403.